The Center for Extended Magnetohydrodynamic Modeling

(Global Stability of Magnetic Fusion Devices)

S. Jardin—lead PI

a SciDAC activity…
Partners with:
TOPS
TSTT
APDEC

MIT: D. Brennan, L. Sugiyama, J. Ramos

NYU: B. Hientzsch, H. Strauss

PPPL: J. Breslau, J. Chen, G. Fu, S. Klasky, W. Park, R. Samtaney

SAIC: D. Schnack, A. Pankin

TechX: S. Kruger

U. Colorado: S. Parker , D. Barnes

U. Wisconsin: J. Callen, C. Hegna, C. Sovinec, C. Kim

U. Utah: A. Sanderson

Utah State: E. Held

CEMM Bibliography for the period 5/04 – 5/05

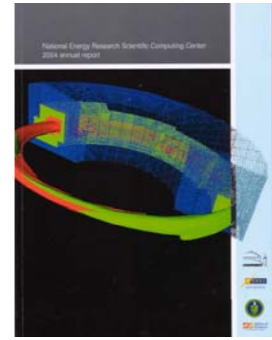

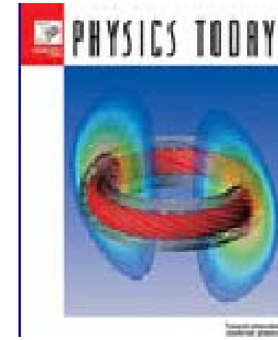

- Strauss, HR; Pletzer, A; Park, W; Jardin, S; Breslau, J; Sugiyama, L. 2004. MHD simulations with resistive wall and magnetic separatrix. *COMPUTER PHYSICS COMMUNICATIONS* 164 (1-3): 40-45.
- Strauss, HR; Sugiyama, LE; Fu, GY; Park, W; Breslau, J. 2004. Simulation of two fluid and energetic particle effects in stellarators. *NUCLEAR FUSION* 44 (9): 1008-1014.
- Chen, J; Breslau, J; Fu, G; Jardin, S; Park, W. 2004. Symmetric solution in M3D. *COMPUTER PHYSICS COMMUNICATIONS* 164 (1-3): 468-471.
- Samtaney, RS; Jardin, SC; Colella, P; Martin, DF. 2004. 3D Adaptive Mesh Refinement simulations of pellet injection in tokamaks. *COMPUTER PHYSICS COMMUNICATIONS* 164 (1-3): 220-228.
- Jardin, SC. 2004. A triangular finite element with first-derivative continuity applied to fusion MHD applications. *JOURNAL OF COMPUTATIONAL PHYSICS* 200 (1): 133-152.
- Jardin, S.C; Breslau, J.A. , 2005, Implicit solution of the four-field extended-magnetohydrodynamic equations using high-order high-continuity finite elements. *PHYSICS OF PLASMAS* 12, 10 pages
- Kruger, SE; Sovinec, CR; Schnack, DD; Held, ED. 2004. Free-boundary simulations of DIII-D plasmas with the NIMROD code. *COMPUTER PHYSICS COMMUNICATIONS* 164 (1-3): 34-39.
- S. E. Kruger, D. D. Schnack, and C. R. Sovinec 2005 Dynamics of the major disruption of a DIII-D plasma, *PHYSICS OF PLASMAS* 12 10-pages
- Wan, W; Chen, Y; Parker, SE. 2005. Gyrokinetic delta f simulation of the collisionless and semicollisional tearing mode instability. *PHYSICS OF PLASMAS* 12 (1): art. no.-012311.
- Kim, CC; Sovinec, CR; Parker, SE. NIMROD Team. 2004. Hybrid kinetic-MHD simulations in general geometry. *COMPUTER PHYSICS COMMUNICATIONS* 164 (1-3): 448-455.
- Sovinec, CR; Cohen, BI; Cone, GA; Hooper, EB; McLean, HS. 2005. Numerical investigation of transients in the SSPX spheromak. *PHYSICAL REVIEW LETTERS* 94 (3): art. no.-035003.
- Held, ED; Callen, JD; Hegna, CC; Sovinec, CR; Gianakon, TA; Kruger, SE. 2004. Nonlocal closures for plasma fluid simulations. *PHYSICS OF PLASMAS* 11 (5): 2419-2426.
- B.I. Cohen, E.B. Hooper, R.H. Cohen, D. N. Hill, H.S. McLean, R.D. Wood, S. Woodruff, C.R. Sovinec, and G.A.Cone, 2005 Simulation of Spheromak evolution and energy confinement, *PHYSICS OF PLASMAS*, 12 9-pages
- J. Ramos, 2005, "Fluid formalism for collisionless magnetized plasmas", *PHYSICS OF PLASMAS* 12 .
- J. Chen, S. C. Jardin, and H.R. Strauss, "Solving Anisotropic Transport Equations on Misaligned Grids", Springer-Verlag, Lecture Notes in Computer Science, 3516, pp. 1076-1079, 2005

Activity Areas

- Spatial Discretizations
  - M3D C^1
  - Spectral and lumped mass elements
- Two-Fluid MHD and Associated Temporal Differencing
- Numerical Closures
- Sawtooth Modeling
- ELM Modeling
- Hybrid Calculations
- Adaptive Mesh Refinement
- Spheromak Modeling
- 2-fluid NSTX Modeling
- Visualization
- Misc.

2D 6-field 2-fluid model has been implemented in M3D-C^1

$$\frac{\partial \vec{B}}{\partial t} = -\nabla \times \vec{E}, \qquad \vec{J} = \nabla \times \vec{B}$$

$$\vec{E} + \vec{V} \times \vec{B} = \frac{1}{ne}\left(\vec{R} + \vec{J} \times \vec{B} - \nabla p_e - \nabla \bullet \overleftrightarrow{\Pi}_e\right)$$

$$nM_i\left(\frac{\partial \vec{V}}{\partial t} + \vec{V} \bullet \nabla \vec{V}\right) + \nabla p_e = \vec{J} \times \vec{B} - \nabla \bullet \overleftrightarrow{\Pi}_i$$

$$\frac{3}{2}\frac{\partial p_e}{\partial t} + \nabla \bullet \left(\frac{3}{2} p_e \vec{V}\right) = -p_e \nabla \bullet \vec{V} + \frac{\vec{J}}{ne} \bullet \left[\frac{3}{2}\nabla p_e + \vec{R} - \nabla \bullet \overleftrightarrow{\Pi}_e\right]$$

$$\vec{V} = \nabla U \times \hat{z} + \nabla_\perp \chi + V_z \hat{z},$$

$$\vec{B} = \nabla \psi \times \hat{z} + I \hat{z}$$

$$p_e$$

$$\vec{R} = \eta n e \vec{J}$$

$$\overleftrightarrow{\Pi}_i = -\mu n\left[\nabla \vec{V} + \nabla \vec{V}^\dagger\right] + h\mu n \nabla^2\left[\nabla \vec{V} + \nabla \vec{V}^\dagger\right]$$

$$\overleftrightarrow{\Pi}_e = \lambda n e\left[\nabla \vec{J} + \nabla \vec{J}^\dagger\right]$$

. take projections of momentum eqn:

$-\hat{z} \cdot \nabla \times$

$\hat{z} \cdot$

$\nabla \bullet$

. expand in C^1 finite elements

. full implicit time differencing

M3D-C^1 code has full Extended MHD (2-fluid) equations with implicit differencing that allows time step to be determined by accuracy only:

$$\vec{V} = \nabla U \times \hat{z} + \nabla_\perp \chi + V_z$$
$$\vec{B} = \nabla \psi \times \hat{z} + I \hat{z}$$

Equations expressed in a form that allows non-trivial subsets of lower rank equations:

$$\begin{bmatrix} S_{11}^v & S_{12}^v & S_{13}^v \\ S_{21}^v & S_{22}^v & S_{23}^v \\ S_{31}^v & S_{32}^v & S_{33}^v \end{bmatrix} \bullet \begin{bmatrix} U \\ V_z \\ \chi \end{bmatrix}^{n+1} = \begin{bmatrix} D_{11}^v & D_{12}^v & D_{13}^v \\ D_{21}^v & D_{22}^v & D_{23}^v \\ D_{31}^v & D_{32}^v & D_{33}^v \end{bmatrix} \bullet \begin{bmatrix} U \\ V_z \\ \chi \end{bmatrix}^{n} + \begin{bmatrix} R_{11}^v & R_{12}^v & R_{13}^v \\ R_{21}^v & R_{22}^v & R_{23}^v \\ R_{31}^v & R_{32}^v & R_{33}^v \end{bmatrix} \bullet \begin{bmatrix} \psi \\ I \\ T_e \end{bmatrix}^{n}$$

Alfven Wave physics

$$\begin{bmatrix} S_{11}^p & S_{12}^p & S_{13}^p \\ S_{21}^p & S_{22}^p & S_{23}^p \\ S_{31}^p & S_{32}^p & S_{33}^p \end{bmatrix} \bullet \begin{bmatrix} \psi \\ I \\ T_e \end{bmatrix}^{n+1} = \begin{bmatrix} D_{11}^p & D_{12}^p & D_{13}^p \\ D_{21}^p & D_{22}^p & D_{23}^p \\ D_{31}^p & D_{32}^p & D_{33}^p \end{bmatrix} \bullet \begin{bmatrix} \psi \\ I \\ T_e \end{bmatrix}^{n} + \begin{bmatrix} R_{11}^p & R_{12}^p & R_{13}^p \\ R_{21}^p & R_{22}^p & R_{23}^p \\ R_{31}^p & R_{32}^p & R_{33}^p \end{bmatrix} \bullet \begin{bmatrix} U \\ V_z \\ \chi \end{bmatrix}^{n+1} + \begin{bmatrix} Q_{11}^p & Q_{12}^p & Q_{13}^p \\ Q_{21}^p & Q_{22}^p & Q_{23}^p \\ Q_{31}^p & Q_{32}^p & Q_{33}^p \end{bmatrix} \bullet \begin{bmatrix} U \\ V_z \\ \chi \end{bmatrix}^{n}$$

Whistler, KAW, field diffusion physics

Phase-I: Reduced 2-field MHD:

$$\frac{\partial}{\partial t}\nabla^2 U + \left[\nabla^2 U, U\right] - \left[\nabla^2\psi, \psi\right] = \mu\nabla^4 U$$
$$\frac{\partial \psi}{\partial t} + \left[\psi, U\right] = \eta\nabla^2\psi$$

Phase-II: Fitzpatrick-Porcelli 4-field model:

$$\frac{\partial}{\partial t}\nabla^2 U = \left[U, \nabla^2 U\right] + \left[\nabla^2\psi, \psi\right] + \mu\nabla^4 U$$
$$\frac{\partial V_z}{\partial t} = \left[U, V_z\right] + c_\beta\left[I, \psi\right] + \mu\nabla^2 V_z$$
$$\frac{\partial \psi}{\partial t} = \left[U, \psi\right] + d_\beta\left[\psi, I\right] + \eta\nabla^2\psi$$
$$\frac{\partial I}{\partial t} = \left[U, I\right] + d_\beta\left[\nabla^2\psi, \psi\right] + c_\beta\left[V_z, \psi\right] + c_\beta^2\eta\nabla^2 I$$

Non-linear evolution of tilting cylinder in full 6-field 2-fluid model

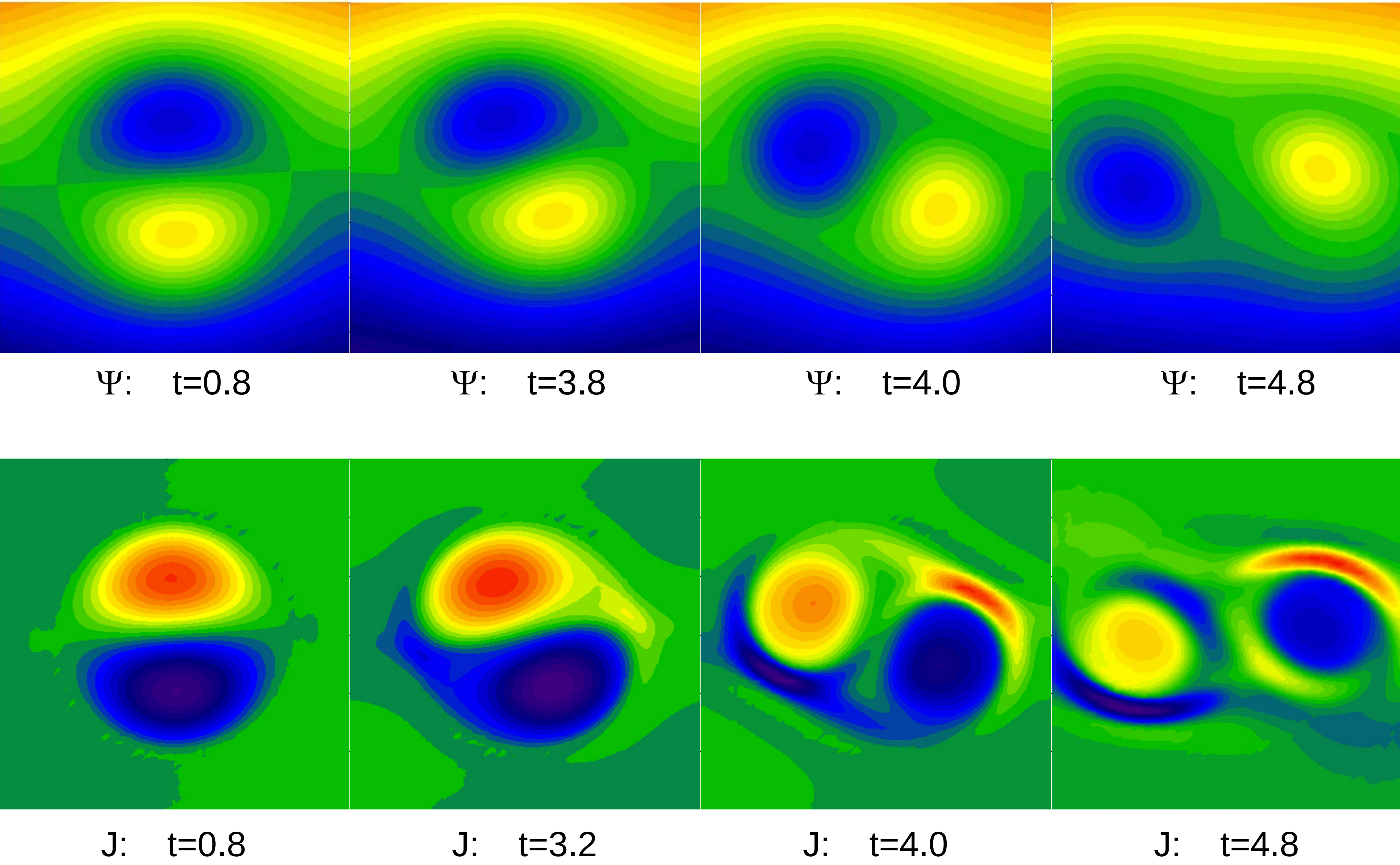

Linear eigenmode of tilting cylinder in 6-field 2-fluid model

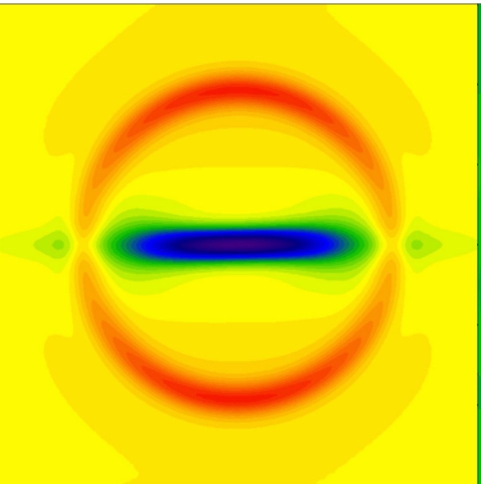

$\nabla^2 U$
Vorticity

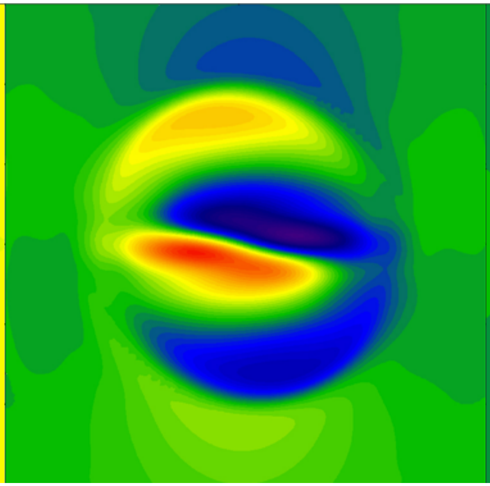

V
Toroidal Velocity

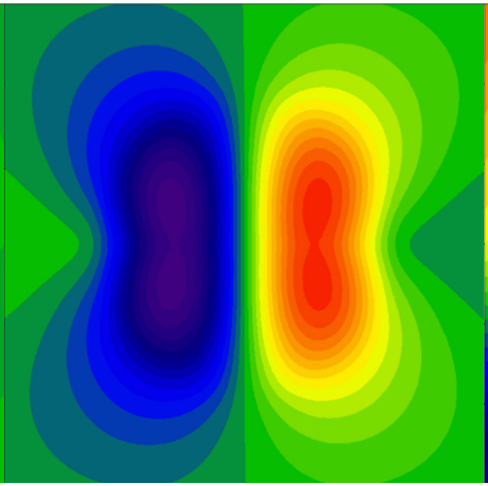

Ψ
Poloidal Flux

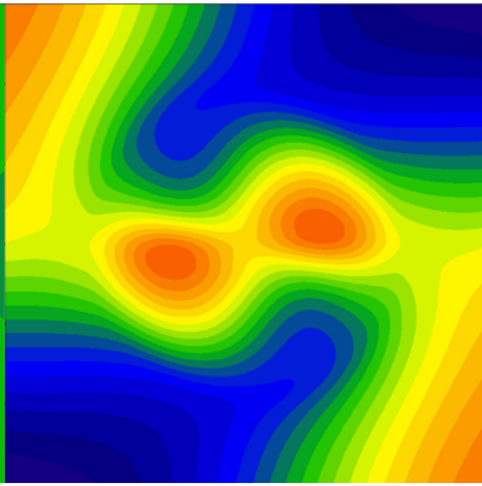

χ
Velocity Potential

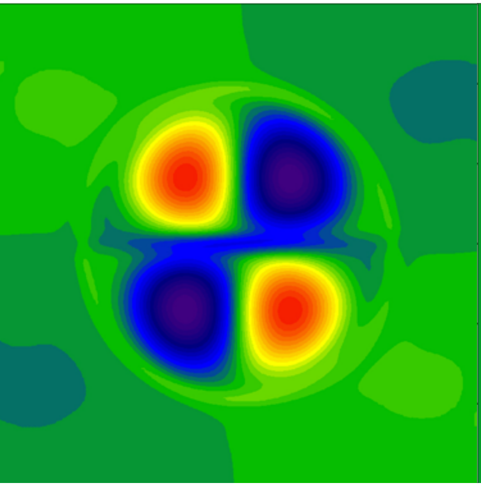

I
Toroidal field

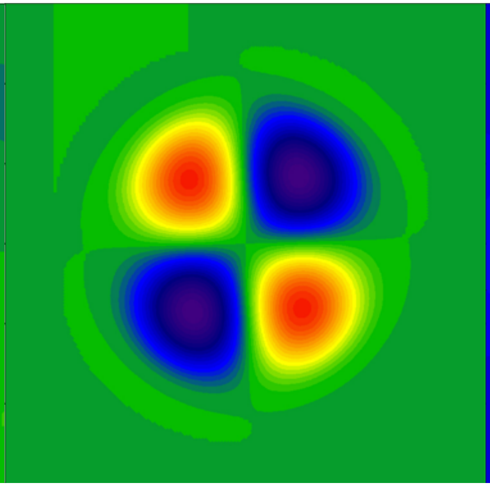

P_e
Electron Pressure

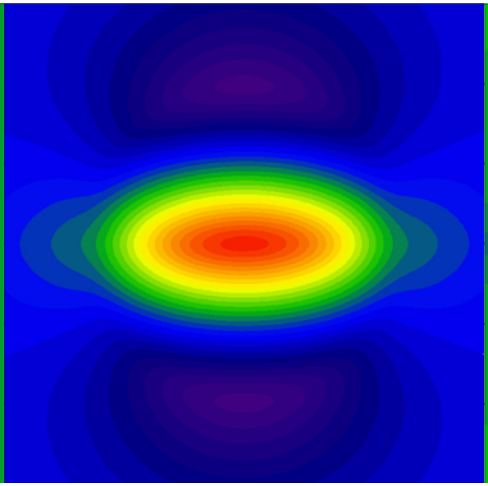

U
Stream Function

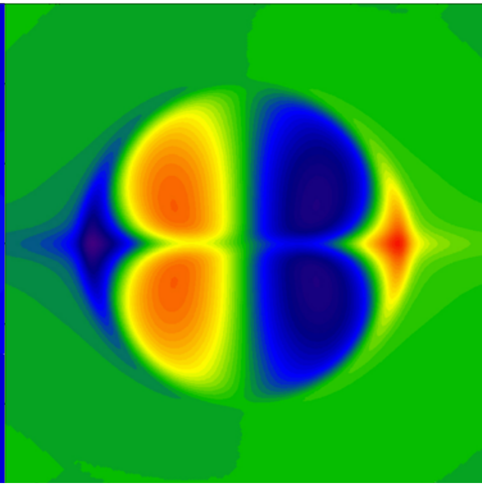

J
Toroidal Current

Braginskii gyro-viscosity:

$$\nabla\cdot\vec{\Pi}=\left\{\left[\nabla\times\left(\frac{mp}{eB^2}\vec{B}\right)\right]\cdot\nabla\right\}\vec{V}-\nabla\left[\frac{mp}{2eB^2}\vec{B}\cdot\left(\nabla\times\vec{V}\right)\right]-\nabla\times\left\{\frac{mp}{eB^2}\left[(B\cdot\nabla)\vec{V}+\frac{1}{2}\left(\nabla\cdot\vec{V}-\frac{3}{B^2}\vec{B}\cdot\left[\left(\vec{B}\cdot\nabla\right)\vec{V}\right]\right)\vec{B}\right]\right\}$$

$$+(B\cdot\nabla)\left\{\frac{mp}{eB^2}\left(\frac{3}{B^2}\vec{B}\times\left[\left(\vec{B}\cdot\nabla\right)\vec{V}\right]+\frac{3}{2B^2}\left[\vec{B}\cdot\left(\nabla\times\vec{V}\right)\right]\vec{B}-\nabla\times\vec{V}\right)\right\}$$

Ramos

$$\hat{z}\cdot\quad\rightarrow\quad[V_z,\alpha I]-\alpha\left\{\left[\psi,\nabla_\perp^2U\right]+\left[\frac{\partial\psi}{\partial x},\frac{\partial U}{\partial x}-\frac{\partial\chi}{\partial y}\right]+\left[\frac{\partial\psi}{\partial y},\frac{\partial U}{\partial y}+\frac{\partial\chi}{\partial x}\right]\right\}-\frac{\partial\alpha}{\partial x}\left[\psi,\frac{\partial U}{\partial x}-\frac{\partial\chi}{\partial y}\right]-\frac{\partial\alpha}{\partial y}\left[\psi,\frac{\partial U}{\partial y}+\frac{\partial\chi}{\partial x}\right]$$

$$+\frac{1}{2}\alpha\nabla_\perp^2\chi\nabla_\perp^2\psi+\frac{1}{2}\left(\alpha\nabla_\perp^2\chi,\psi\right)-\frac{1}{2}\left[(\gamma\kappa,\psi)+\gamma\kappa\nabla_\perp^2\psi\right]+[\gamma\xi_z,\psi]+\frac{1}{2}[\lambda I,\psi]+\left[\alpha\nabla_\perp^2U,\psi\right]$$

$$-\hat{z}\cdot\nabla\times\quad\rightarrow\quad\left[\frac{\partial\chi}{\partial x}+\frac{\partial U}{\partial y},\frac{\partial(\alpha I)}{\partial y}\right]-\left[\frac{\partial\chi}{\partial y}-\frac{\partial U}{\partial x},\frac{\partial(\alpha I)}{\partial x}\right]+\left[\nabla_\perp^2U,\alpha I\right]+\nabla_\perp^2\left\{\alpha[\psi,V_z]\right\}-\frac{1}{2}\nabla_\perp^2\left(\alpha I\nabla_\perp^2\chi\right)+\frac{1}{2}\nabla_\perp^2(\gamma\kappa I)$$

$$+\frac{\partial}{\partial y}[\gamma\xi_x,\psi]-\frac{\partial}{\partial x}[\gamma\xi_y,\psi]+\frac{1}{2}\left\{\frac{\partial\lambda}{\partial x}\left[\frac{\partial\psi}{\partial x},\psi\right]+\frac{\partial\lambda}{\partial y}\left[\frac{\partial\psi}{\partial y},\psi\right]+([\lambda,\psi],\psi)+\left[\lambda\nabla_\perp^2\psi,\psi\right]\right\}+\frac{\partial}{\partial x}\left[\psi,\alpha\frac{\partial V_z}{\partial x}\right]+\frac{\partial}{\partial y}\left[\psi,\alpha\frac{\partial V_z}{\partial y}\right]$$

$$\nabla\cdot\quad\rightarrow\quad\left[\frac{\partial\chi}{\partial x}+\frac{\partial U}{\partial y},\frac{\partial(\alpha I)}{\partial x}\right]+\left[\frac{\partial\chi}{\partial y}-\frac{\partial U}{\partial x},\frac{\partial(\alpha I)}{\partial y}\right]+\left[\nabla_\perp^2\chi,\alpha I\right]+\frac{1}{2}\nabla_\perp^2\left\{\alpha\left[I\nabla_\perp^2U-(\psi,V_z)\right]\right\}+\frac{\partial}{\partial x}[\gamma\xi_x,\psi]+\frac{\partial}{\partial y}[\gamma\xi_y,\psi]$$

$$+\frac{1}{2}[[\lambda,\psi],\psi]+\lambda\left[\frac{\partial\psi}{\partial y},\frac{\partial\psi}{\partial x}\right]+\frac{1}{2}\frac{\partial\lambda}{\partial x}\left[\frac{\partial\psi}{\partial y},\psi\right]-\frac{1}{2}\frac{\partial\lambda}{\partial y}\left[\frac{\partial\psi}{\partial x},\psi\right]+\frac{\partial}{\partial x}\left\{\alpha\left[\psi,\frac{\partial V_z}{\partial y}\right]\right\}-\frac{\partial}{\partial y}\left\{\alpha\left[\psi,\frac{\partial V_z}{\partial x}\right]\right\}+[V_z,[\alpha,\psi]]$$

$$\alpha\equiv\frac{ep}{mB^2}=\frac{ep/m}{\left(\frac{\partial\psi}{\partial x}\right)^2+\left(\frac{\partial\psi}{\partial y}\right)^2+I^2}$$

$$\gamma=\frac{3ep/m}{\left[\left(\frac{\partial\psi}{\partial x}\right)^2+\left(\frac{\partial\psi}{\partial y}\right)^2+I^2\right]^2}$$

$$\vec{\xi}=\left\{\frac{\partial\psi}{\partial x}[\psi,V_z]+I\left[\psi,\frac{\partial\chi}{\partial y}-\frac{\partial U}{\partial x}\right]\right\}\hat{x}+\left\{\frac{\partial\psi}{\partial y}[\psi,V_z]-I\left[\psi,\frac{\partial\chi}{\partial x}+\frac{\partial U}{\partial y}\right]\right\}\hat{y}-\left\{\frac{\partial\psi}{\partial x}\left[\psi,\frac{\partial\chi}{\partial x}+\frac{\partial U}{\partial y}\right]+\frac{\partial\psi}{\partial y}\left[\psi,\frac{\partial\chi}{\partial y}-\frac{\partial U}{\partial x}\right]\right\}\hat{z}$$

$$\lambda=\gamma\left[(\psi,V_z)-I\nabla_\perp^2U\right]$$

$$\kappa\equiv\frac{\partial\psi}{\partial y}\left[\frac{\partial\chi}{\partial x}+\frac{\partial U}{\partial y},\psi\right]-\frac{\partial\psi}{\partial x}\left[\frac{\partial\chi}{\partial y}-\frac{\partial U}{\partial x},\psi\right]+I[V_z,\psi]$$

Breslau

Activity Areas

- Spatial Discretizations
  - M3D C^1
  - Spectral and Lumped Mass Elements
- Two-Fluid MHD and Associated Temporal Differencing
- Numerical Closures
- Sawtooth Modeling
- ELM Modeling
- Hybrid Calculations
- Adaptive Mesh Refinement
- Spheromak Modeling
- 2-fluid NSTX Modeling
- Visualization
- Misc.

2nd and 3rd order lumped mass elements in M3D

- 2nd or 3rd order lumped mass elements in poloidal plane [Cohen et al, SIAM J. Numer. Anal. 38, 2047-2078 (2001)]
- Nodal points coincide with quadrature points
- Gives diagonal mass matrix ... important for M3D
- Theoretical 3rd (2nd order) and 4th order accuracy
- Now implemented in M3D .. being applied to ELM simulations
- Higher order spectral elements being explored by B. Hientzsch

Nodal points of conventional 2nd order Lagrange element

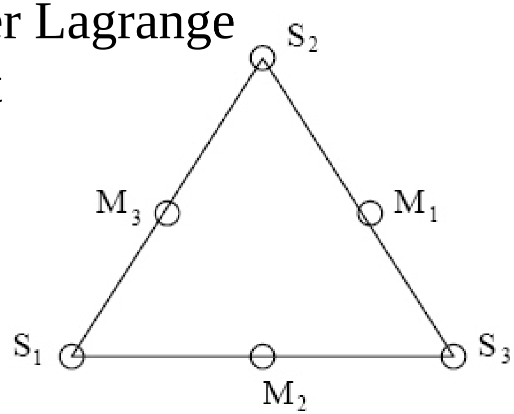

Quadrature Points of Conventional 2nd order element

and

Nodal points And quadrature Points of 2nd order Spectral element

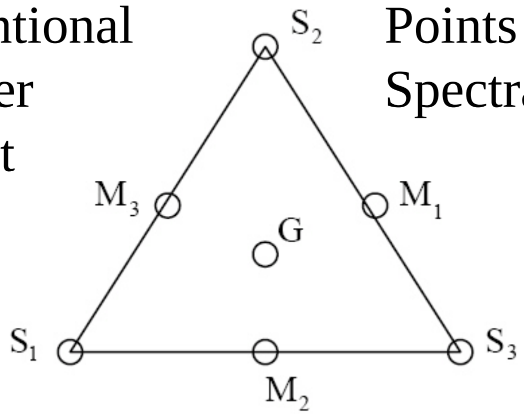

Activity Areas

- Spatial Discretizations
  - M3D C^1
  - Spectral and lumped mass elements
- Two-Fluid MHD and Associated Temporal Differencing
- Numerical Closures
- Sawtooth Modeling
- ELM Modeling
- Hybrid Calculations
- Adaptive Mesh Refinement
- Spheromak Modeling
- 2-fluid NSTX Modeling
- Visualization
- Misc.

A new algorithm uses the leap-frog staggered data representation with a time-centered magnetic field update.

• This approach was motivated by the successful combination of the semi-implicit algorithm and time-centered advection (reported in http://www.cptc.wisc.edu/sovinec_research/meetings/sovinec_aps03poster.pdf)

Neglecting advection, dissipation, and the separate *n* and *T* advances for clarity:

$$\left(\rho+\Delta t^2 L\right)\Delta\mathbf{V}=\left(\Delta t\mathbf{J}^{n+1/2}\times\mathbf{B}^{n+1/2}-\Delta t\nabla p^{n+1/2}\right)$$

$$\Delta p=-\Delta t\gamma\, p^{n+1/2}\nabla\cdot\mathbf{V}^{n+1}$$

$$\Delta\mathbf{B}+\frac{\Delta t}{2}\nabla\times\frac{1}{ne}\left(\mathbf{J}^{n+1/2}\times\Delta\mathbf{B}+\frac{\nabla\times\Delta\mathbf{B}}{\mu_0}\times\mathbf{B}^{n+1/2}\right)=$$
$$\Delta t\nabla\times\left(\mathbf{V}^{n+1}\times\mathbf{B}^{n+1/2}\right)-\Delta t\nabla\times\frac{1}{ne}\left(\mathbf{J}^{n+1/2}\times\mathbf{B}^{n+1/2}-\nabla p_e\right)$$

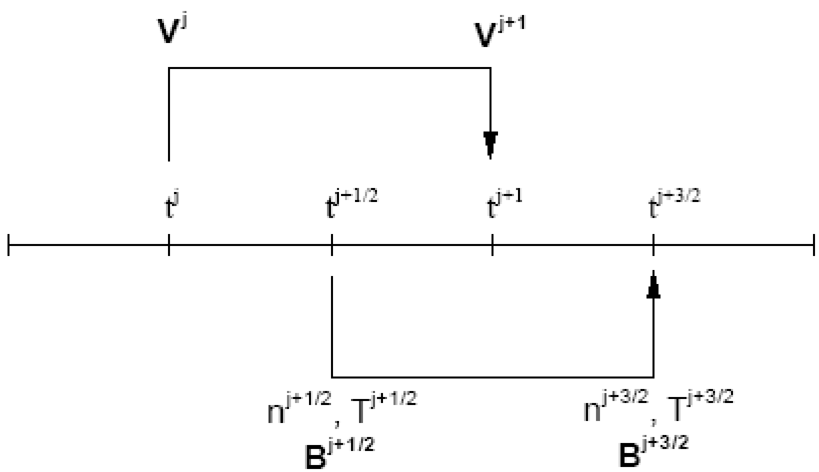

• The implicit Hall terms are linearized from the beginning of a time-step.

Sovinec

NIMROD reproduces fast reconnection in the GEM Challenge problem.

C. Sovinec and H. Tian, UW-Madison

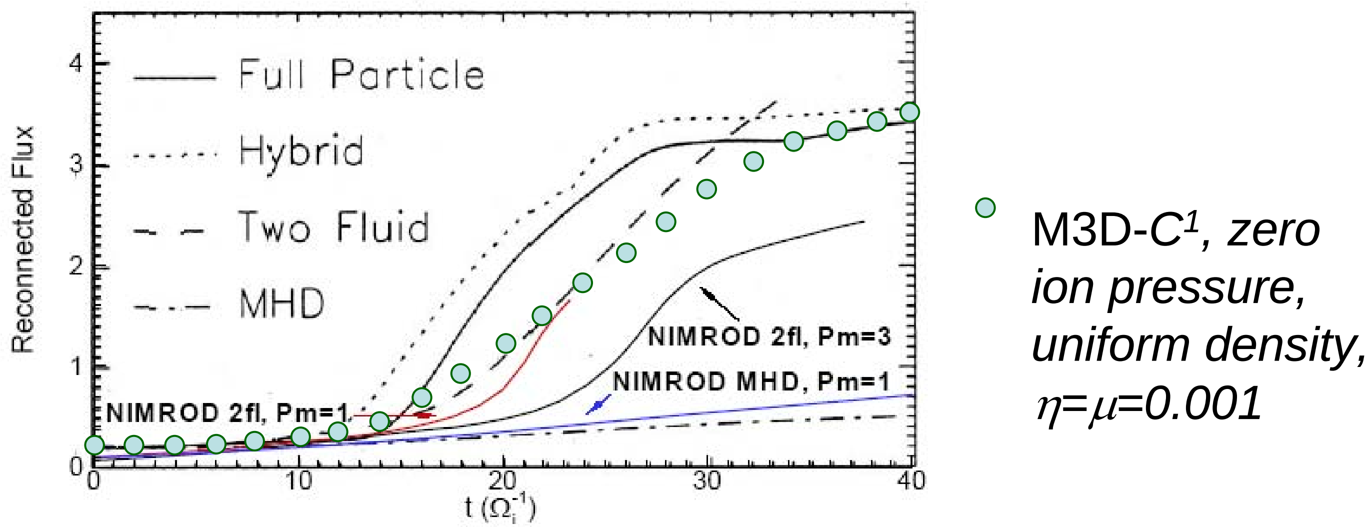

Reconnected magnetic flux in the GEM Challenge problem as a function of time.

- This comparison shows recent NIMROD Hall-MHD and resistive MHD results together with results published in Birn *et al.*, JGR.

- This problem has no guide field, and reconnection generates sonic flows well into the nonlinear phase of the 2-fluid computations.

- Since NIMROD does not have shock-capturing capabilities, viscosity is required. With a 72×96 mesh of biquadratic elements, Pm=3 is required to achieve saturation.

M3D-C^1 61x61 triangles, no symmetry imposed: t=30

GEM Magnetic Reconnection 6-field 2-fluid model: t=30, $V_{MAX} \sim 0.8\ V_A$

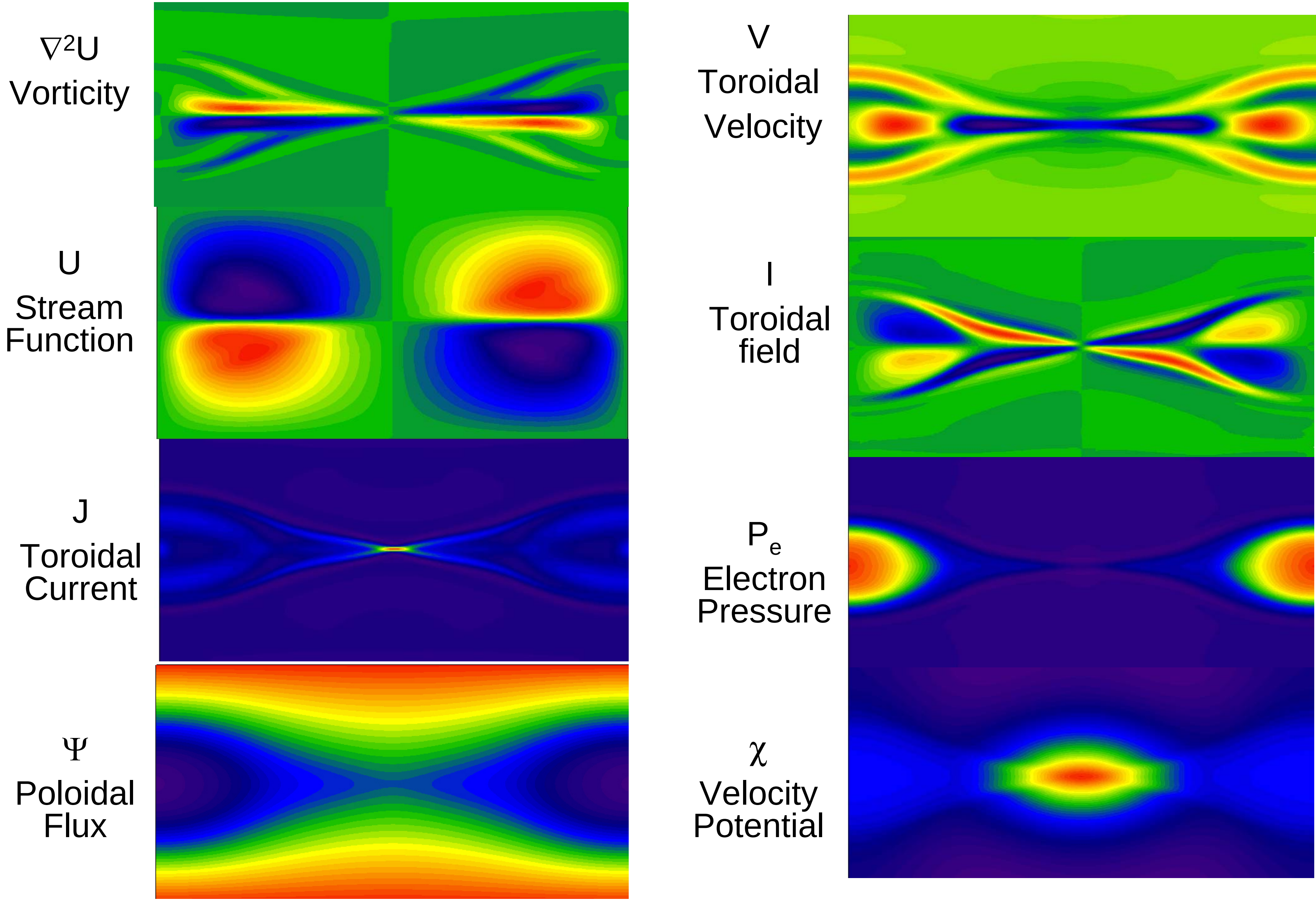

M3D-C^1 61x61 triangles, no symmetry imposed: t=40

GEM Magnetic Reconnection 6-field 2-fluid model: t=40, V_{MAX} ~ 0.8 V_A

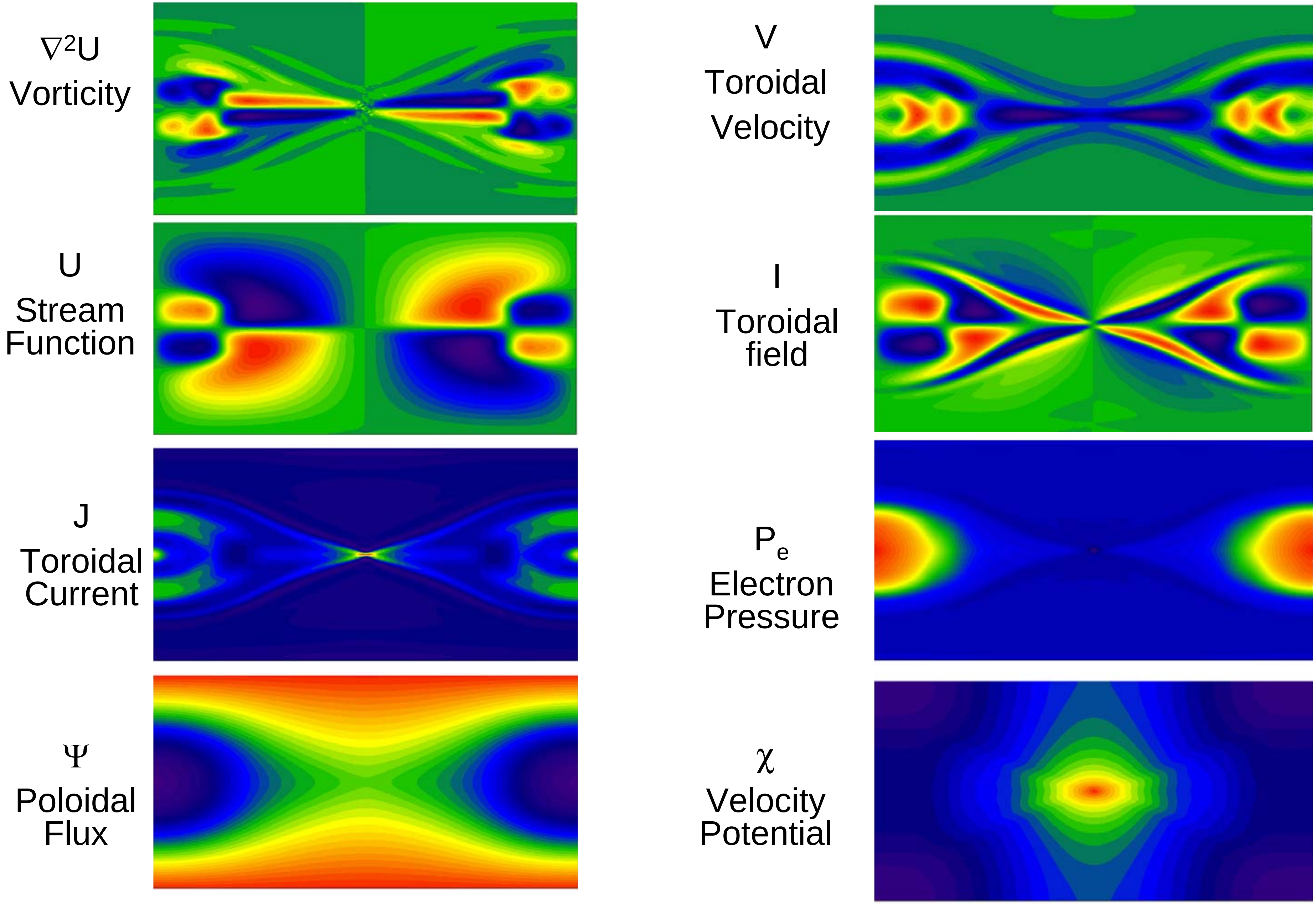

Activity Areas

- Spatial Discretizations
  - M3D C^1
  - Spectral and lumped mass elements
- Two-Fluid MHD and Associated Temporal Differencing
- Numerical Closures
- Sawtooth Modeling
- ELM Modeling
- Hybrid Calculations
- Adaptive Mesh Refinement
- Spheromak Modeling
- 2-fluid NSTX Modeling
- Visualization
- Misc.

Improved efficiency of nonlocal, parallel closure implementation in NIMROD.

- Parallel heat flow, $q_{||}$, and parallel ion stress now calculated by using a Lomb periodogram approach:
  - fit to approximate asymptotic forms of temperature and flow perturbations using data from integrations along magnetic field.
- Previous $q_{||}$ implementation took a week on 256 processors with T = 1 keV.
- Profiles shown at right calculated in 10 minutes on workstation with T = 5 keV.
- Parallel closures ready to handle extreme temperatures and low collisionality of ITER plasmas.

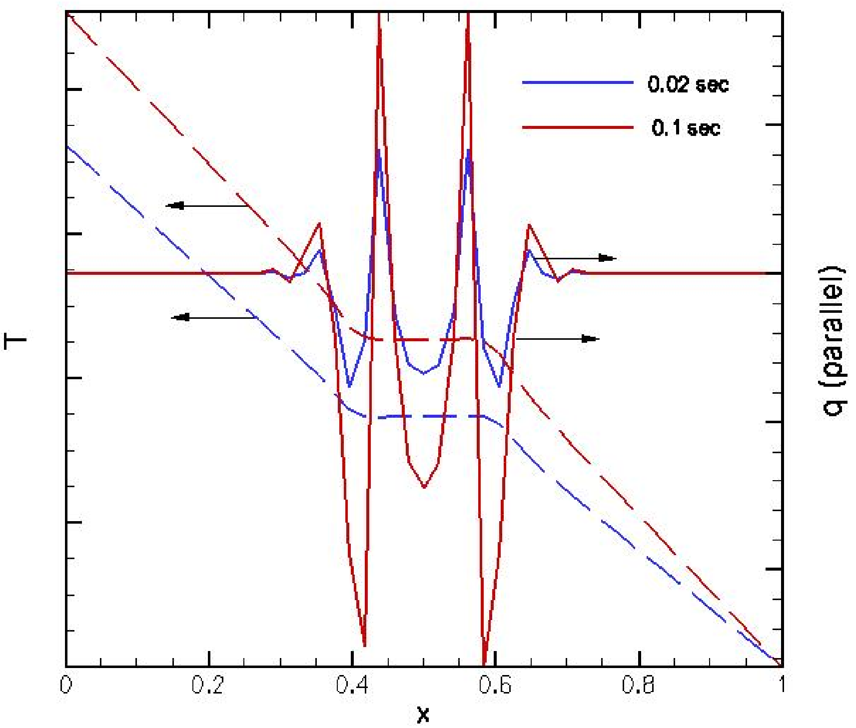

T and $q_{||}$ profiles across slab magnetic island show flattening in T and localized heat flow response. Island is centered at 0.4 < x < 0.6 and T = 5 keV corresponds to a collision length of several kilometers.

Held

Activity Areas

- Spatial Discretizations
  - M3D C^1
  - Spectral and lumped mass elements
- Two-Fluid MHD and Associated Temporal Differencing
- Numerical Closures
- Sawtooth Modeling
- ELM Modeling
- Hybrid Calculations
- Adaptive Mesh Refinement
- Spheromak Modeling
- 2-fluid NSTX Modeling
- Visualization
- Misc.

M3D Poloidal Mesh for CDX

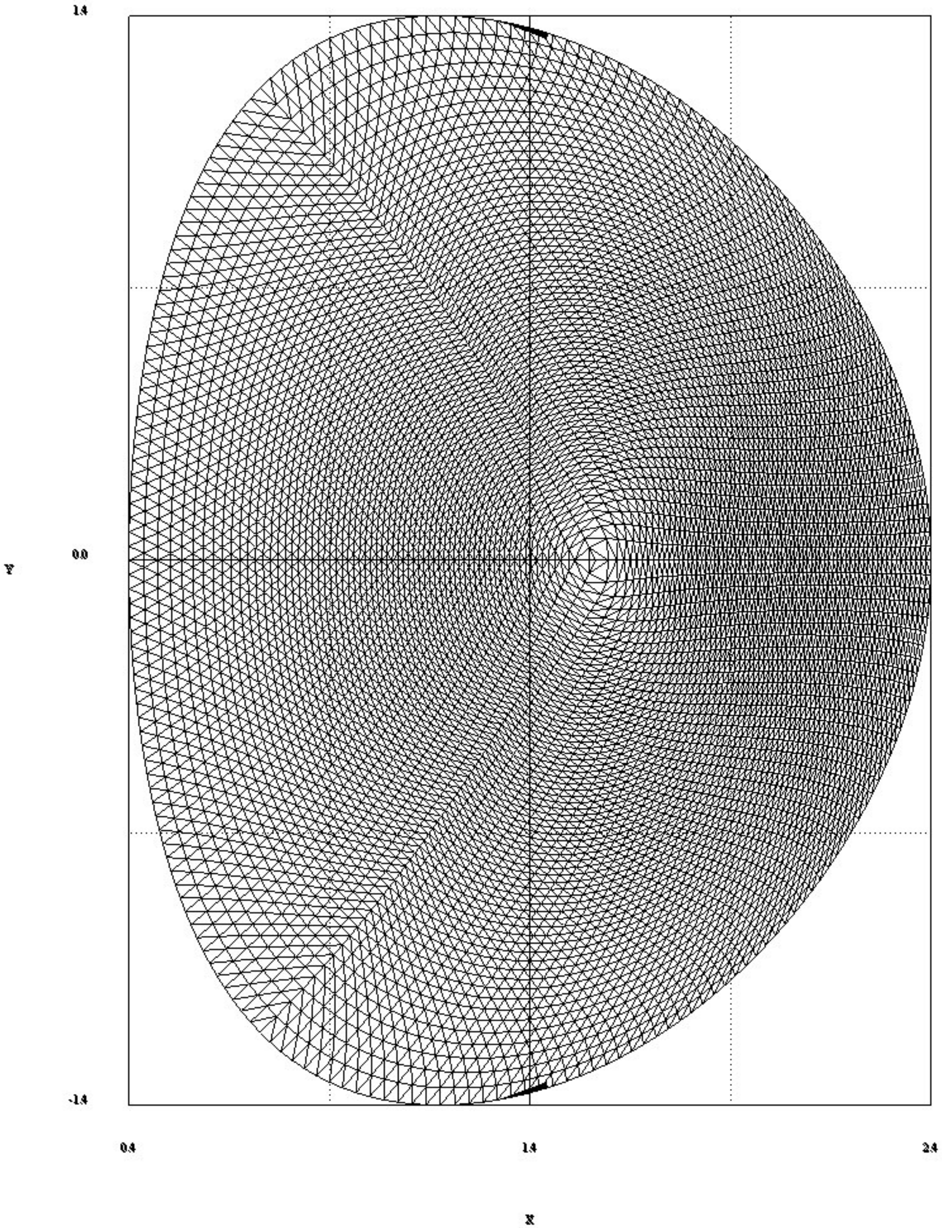

- 89 radial zones, up to 267 in θ in unstructured mesh
- Linear basis functions on triangular elements
- Conducting wall; current drive applied by adding a source term in Ohm’s law.
- Finite differences toroidally; 24 planes

Breslau

n=1 Eigenmode

Incompressible velocity
stream function U

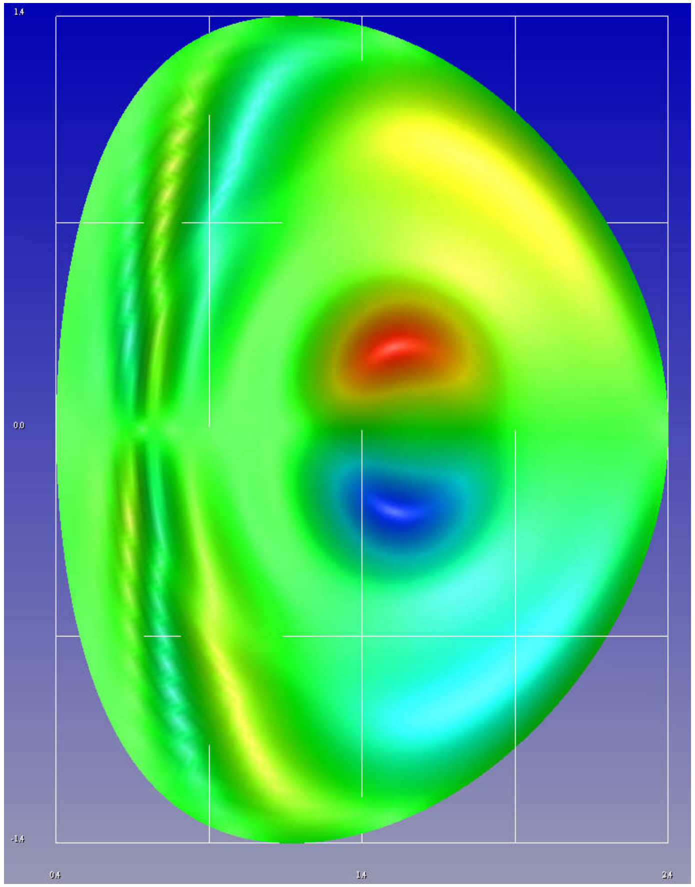

Toroidal current density
J_ϕ

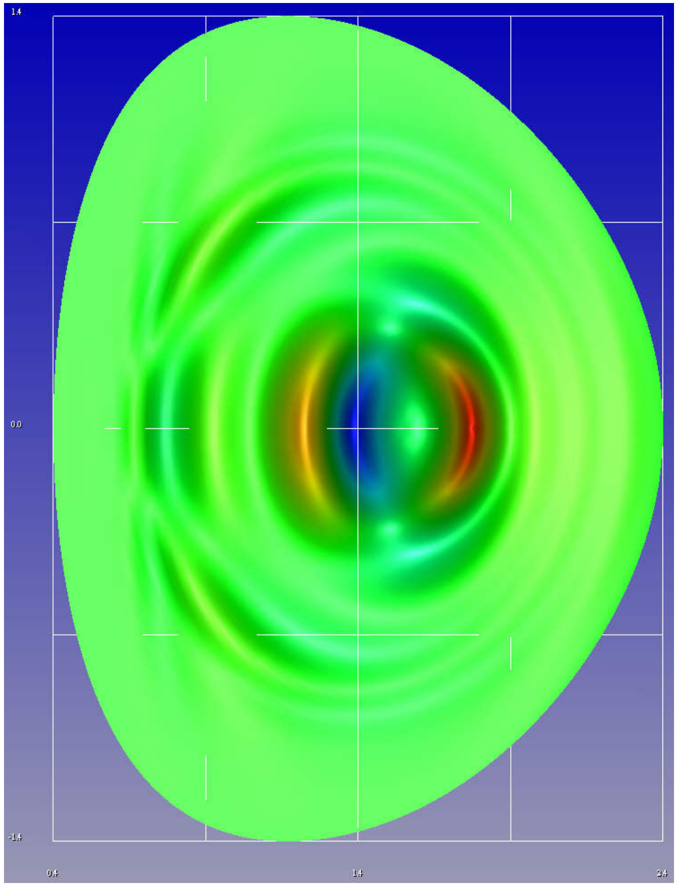

$\gamma\tau_A = 8.61\times 10^{-3} \rightarrow$ growth time = 116 τ_A

Breslau

Higher n Eigenmodes

Incompressible velocity
stream function U

$n = 2$

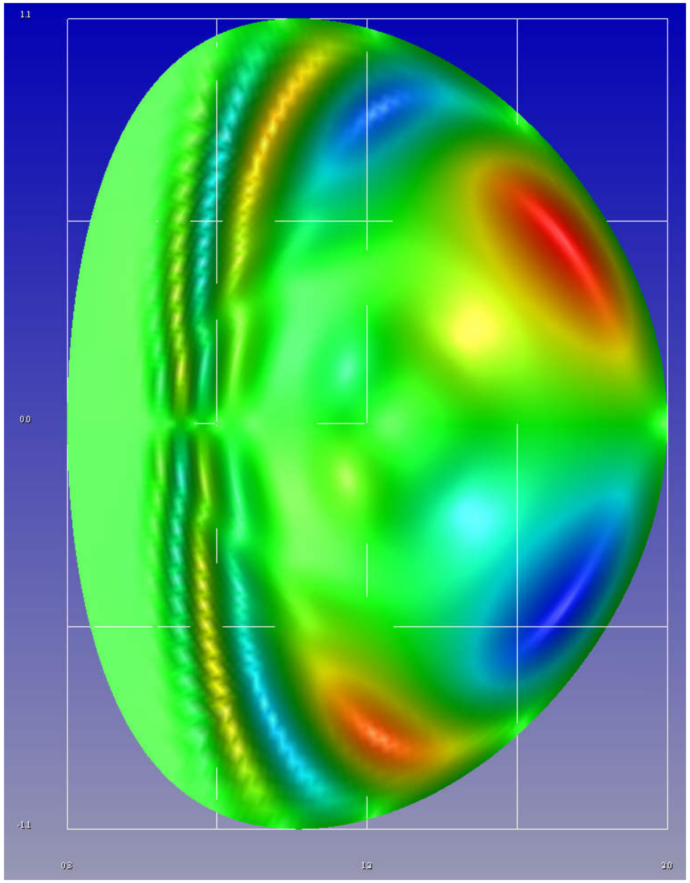

$m \geq 5$
$\gamma \tau_A = 1.28 \times 10^{-2}$

$n = 3$

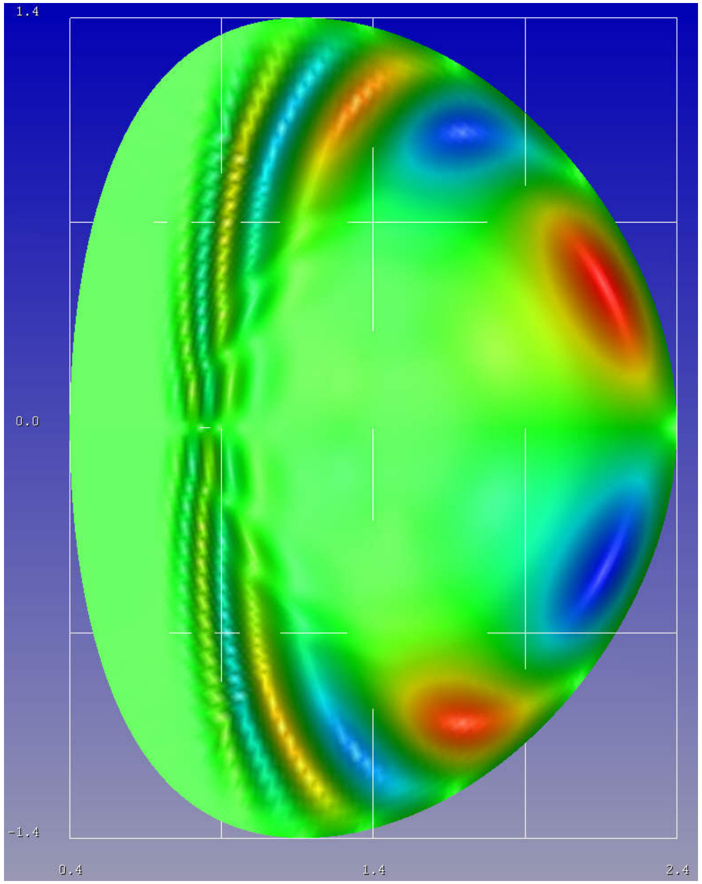

$m \geq 7$
$\gamma \tau_A = 1.71 \times 10^{-2}$

• • •

Breslau

In Absence of Heat Conduction, Higher *n* Resistive Ballooning Modes are More Unstable than Internal Kink

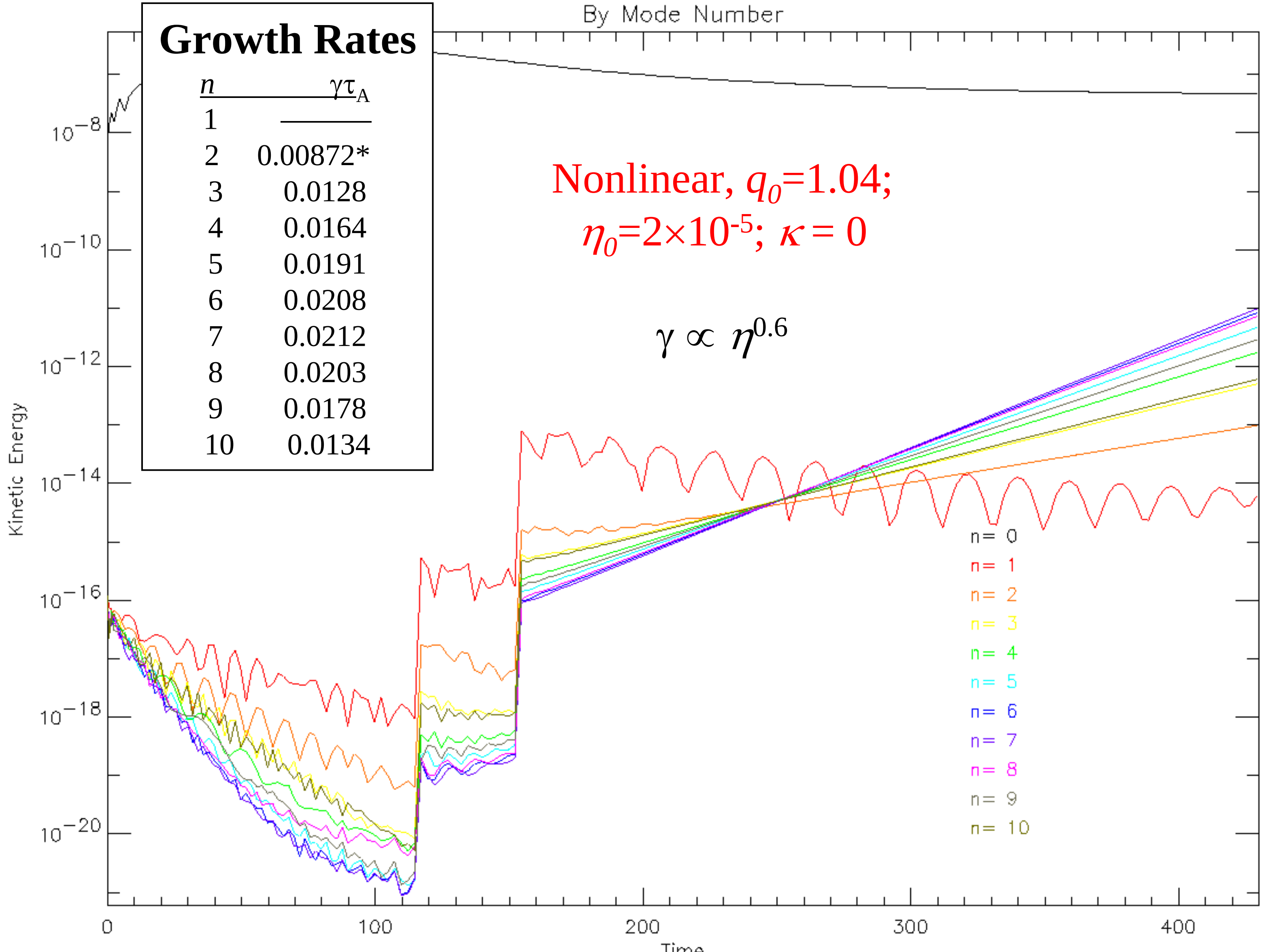

Growth Rates

n	$\gamma\tau_A$
1	———
2	0.00872*
3	0.0128
4	0.0164
5	0.0191
6	0.0208
7	0.0212
8	0.0203
9	0.0178
10	0.0134

Breslau

High Perpendicular Heat Conduction Stabilizes All Resistive Ballooning Modes

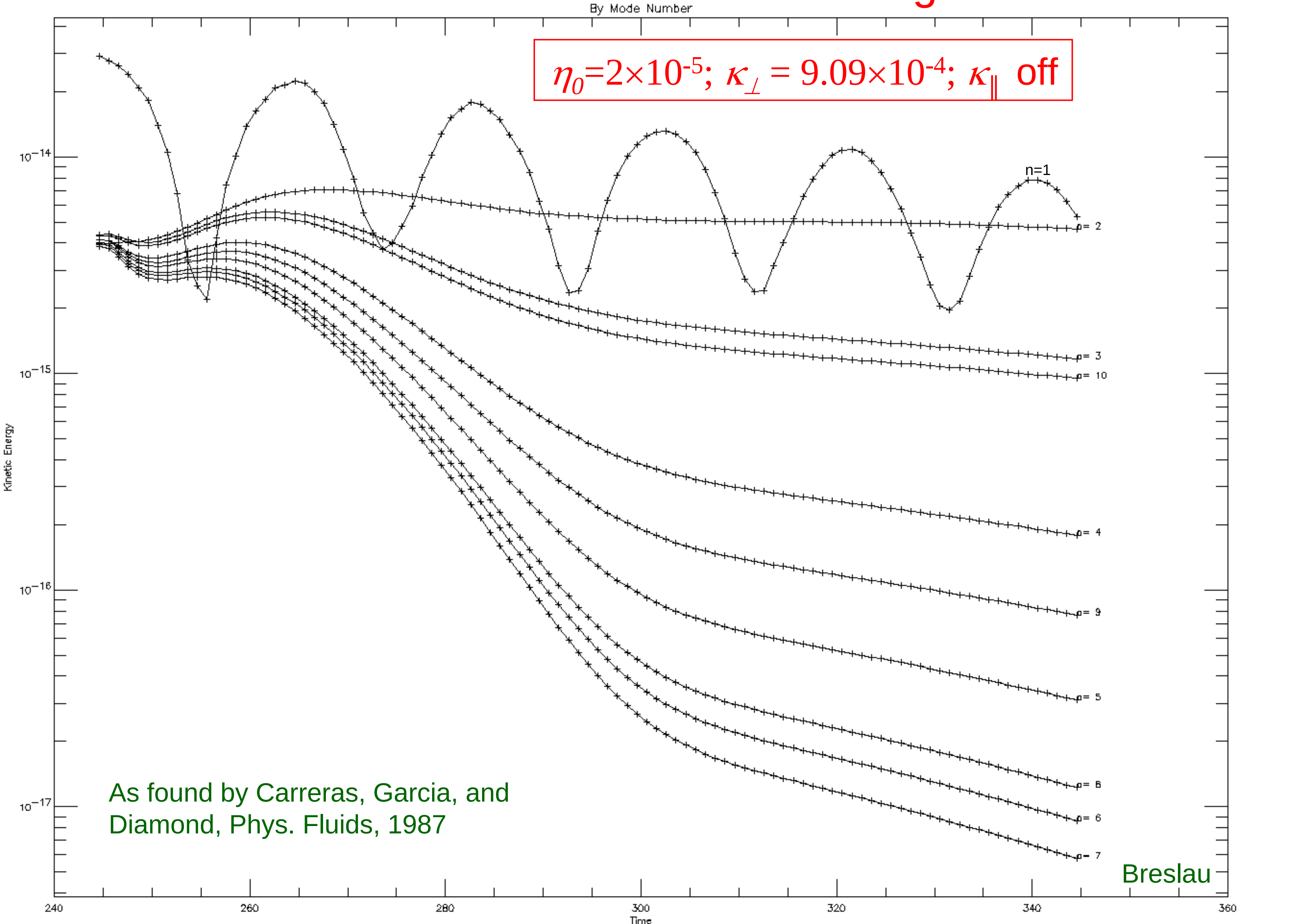

Nonlinear Evolution, Heat Conduction On

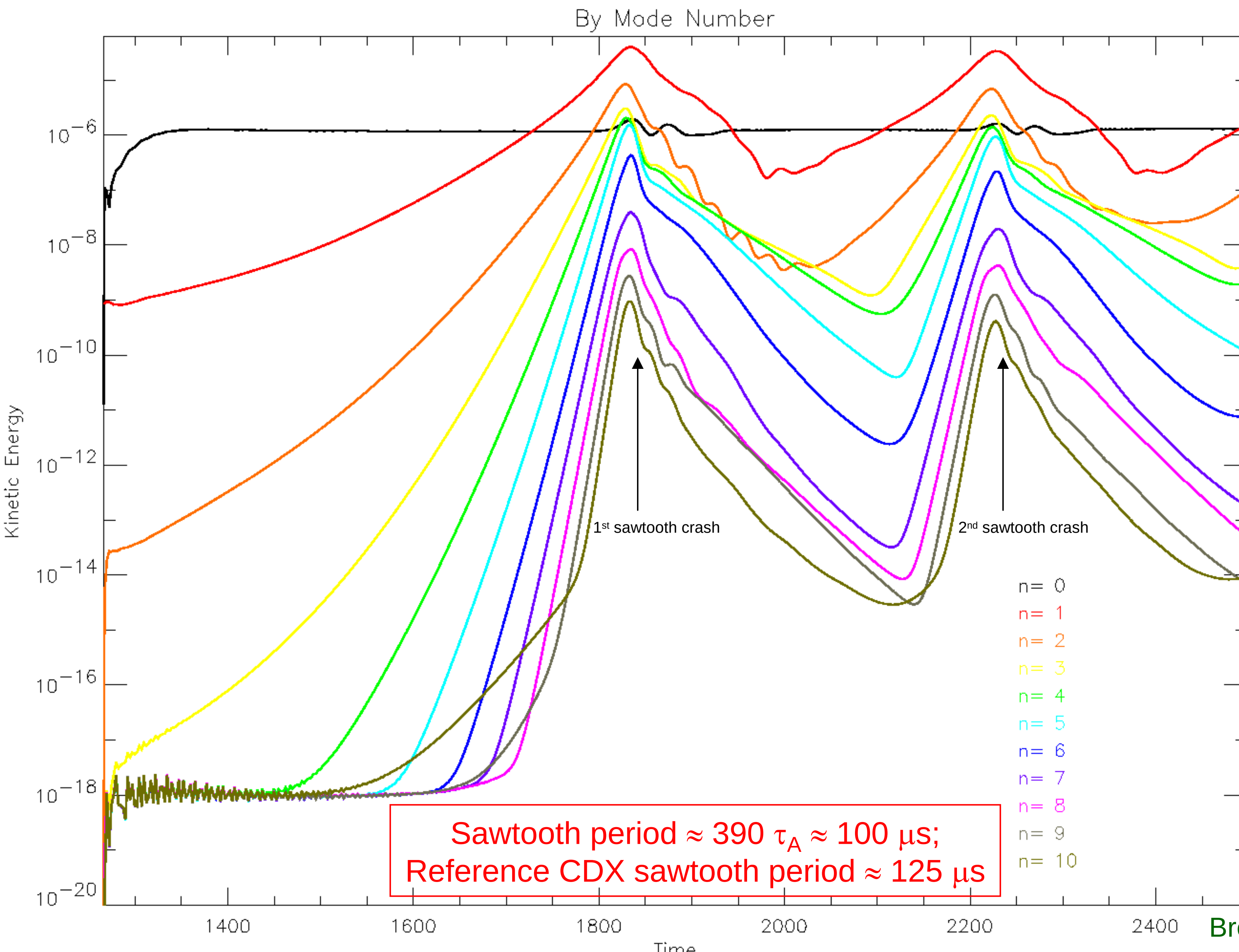

Sawtooth period ≈ 390 τ_A ≈ 100 μs;
Reference CDX sawtooth period ≈ 125 μs

Breslau

M3D field line plots during sawtooth cycles

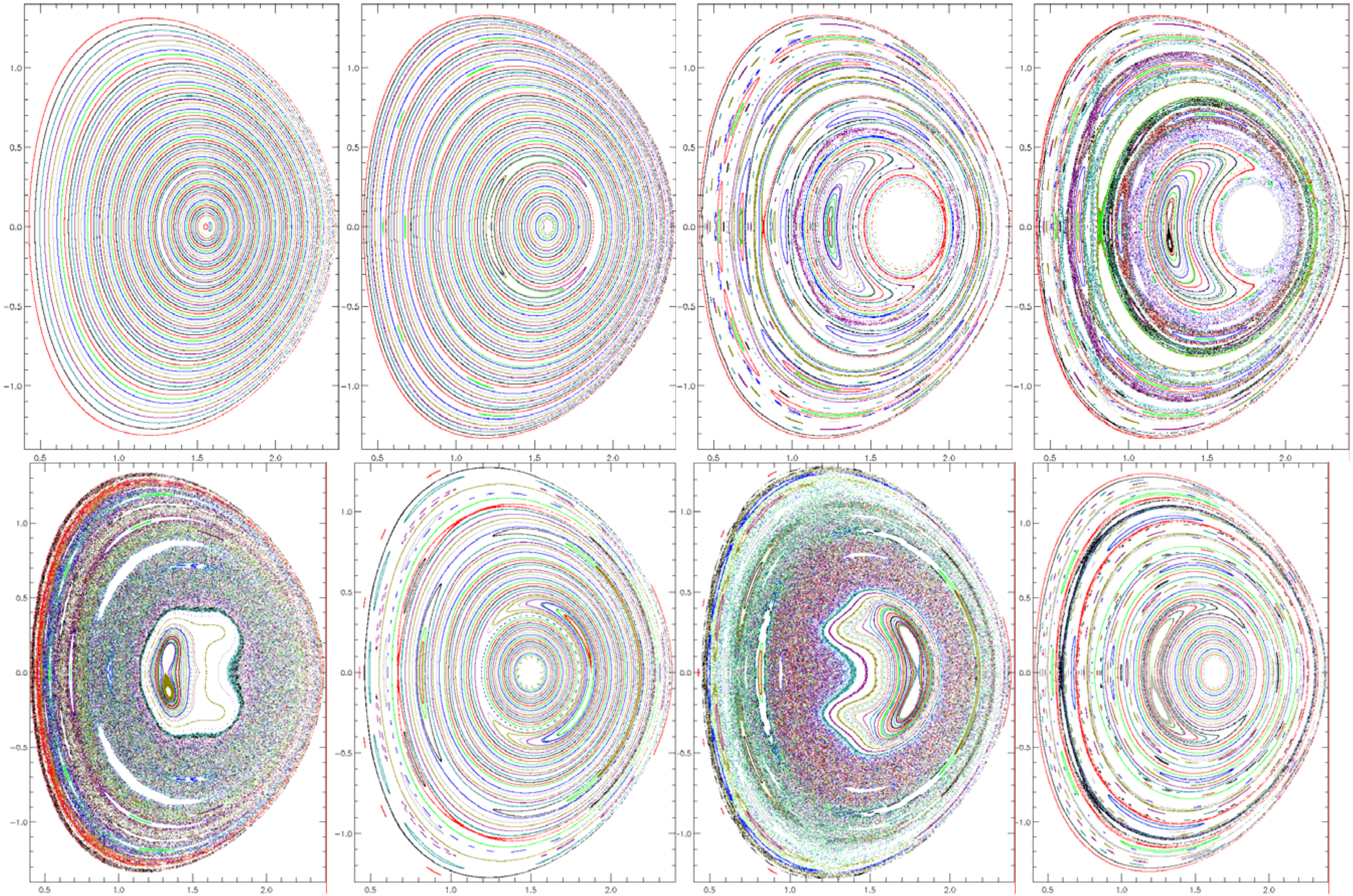

After first crash

After second crash

Breslau

Temperature profiles during CDX-U sawtooth crashes

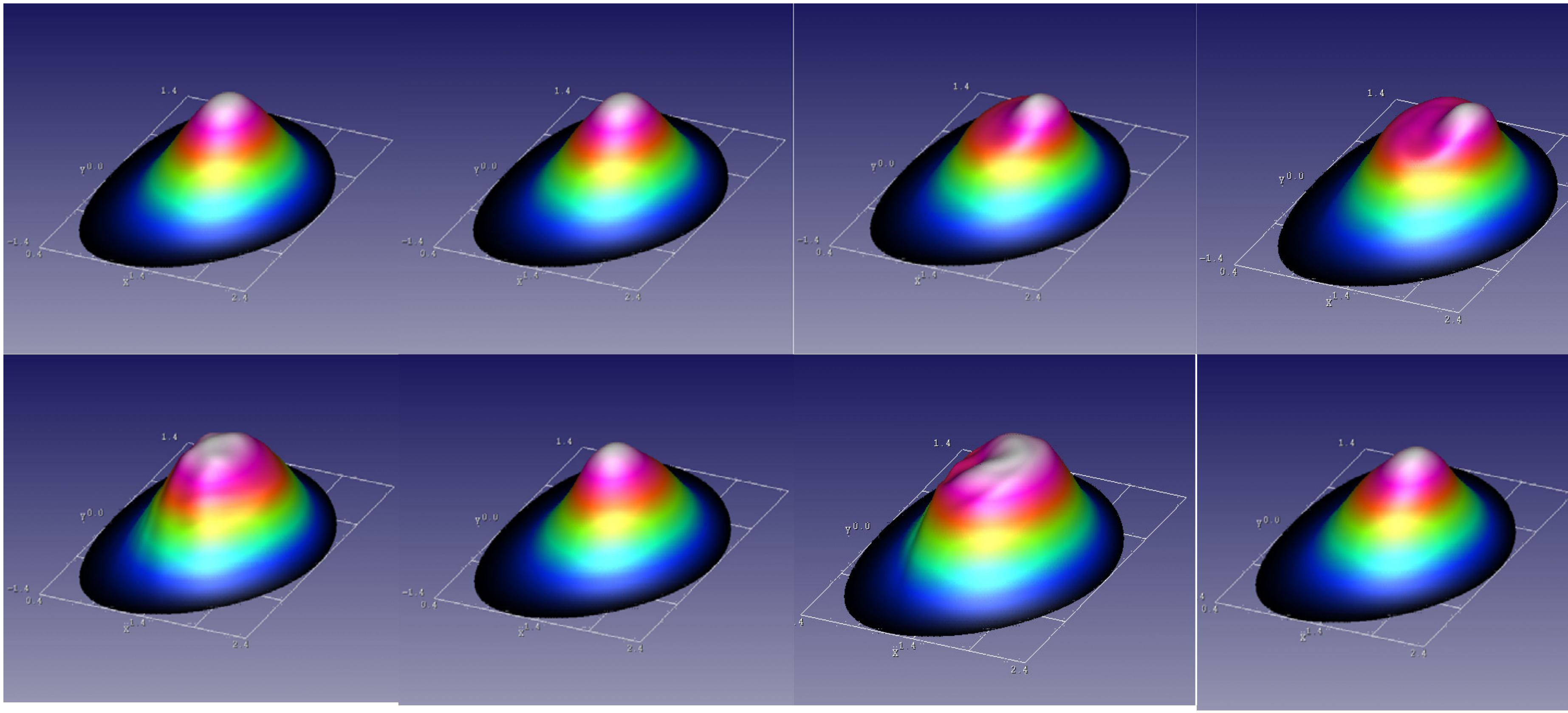

After first crash

After second crash

Breslau
M3D

NIMROD Kinetic energy history

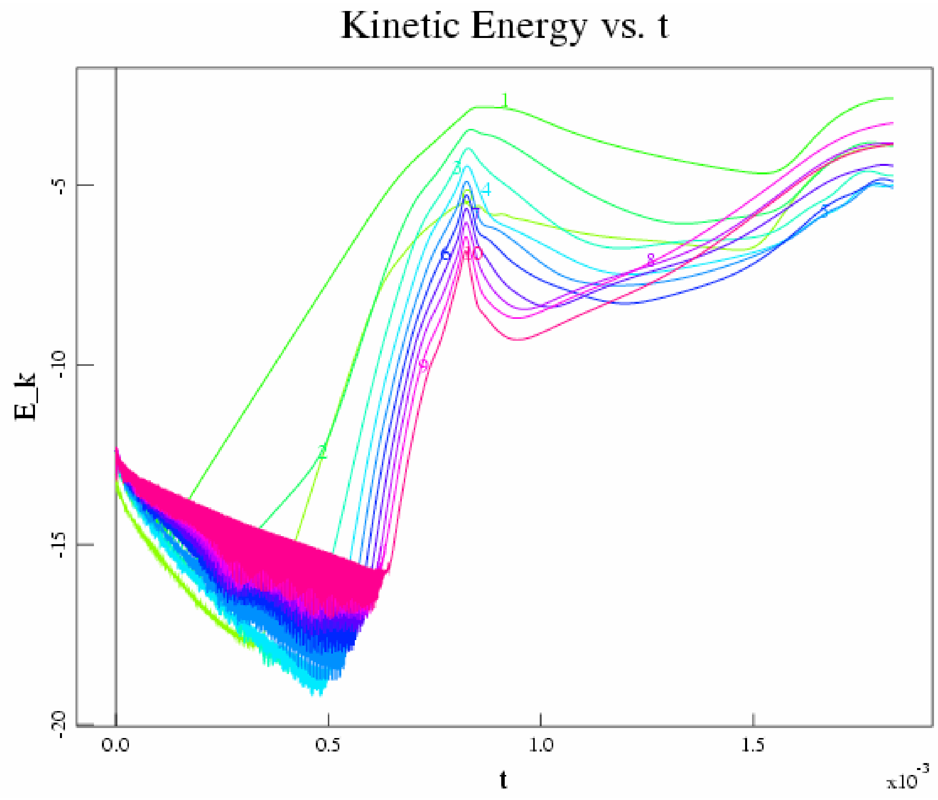

11 modes

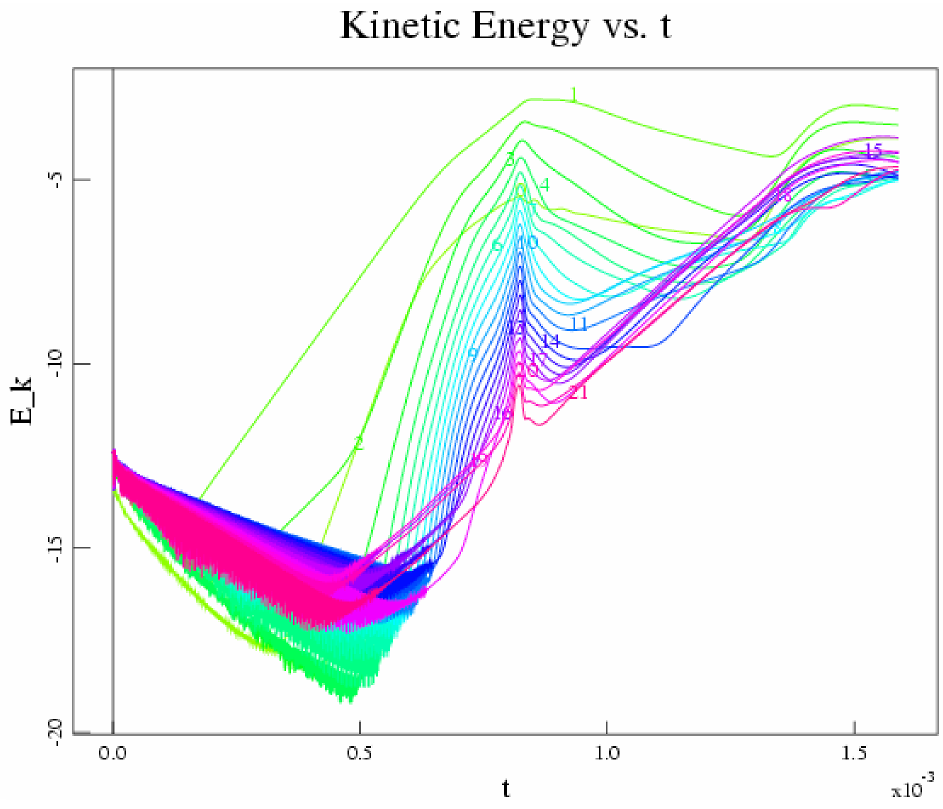

22 modes

- Same initial equilibrium as M3D: linear modes agree
- Large Anisotropic thermal conduction with $k_{||}/ k_{\perp} = 10^8$
- Does <u>not</u> have experimental $k_{\perp} = 200\ m^2/s$

Schnack
Pankin

NIMROD n=1 current density

22 modes

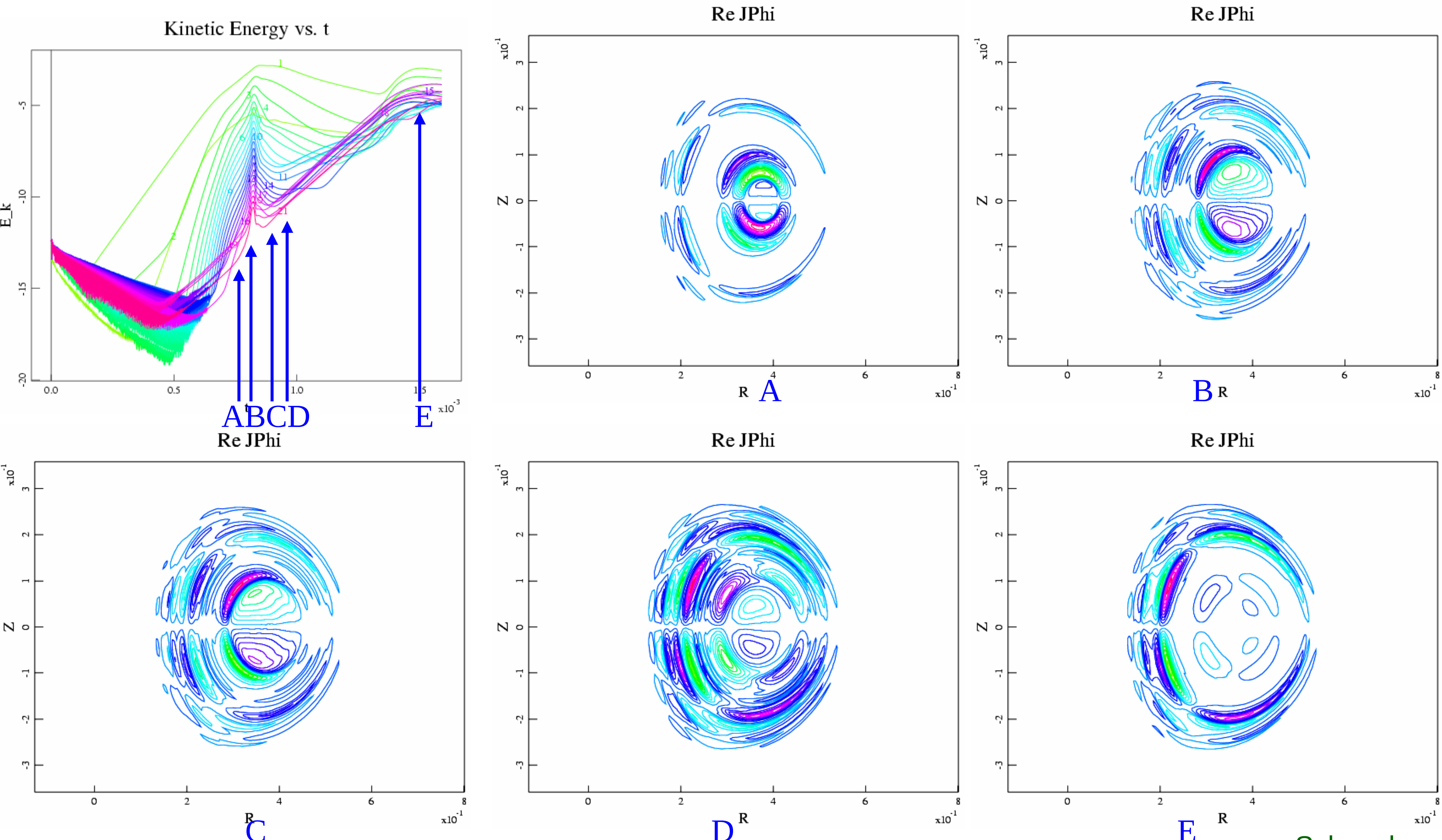

Schnack
Pankin

Poincare plots of NIMROD sawtooth cycle

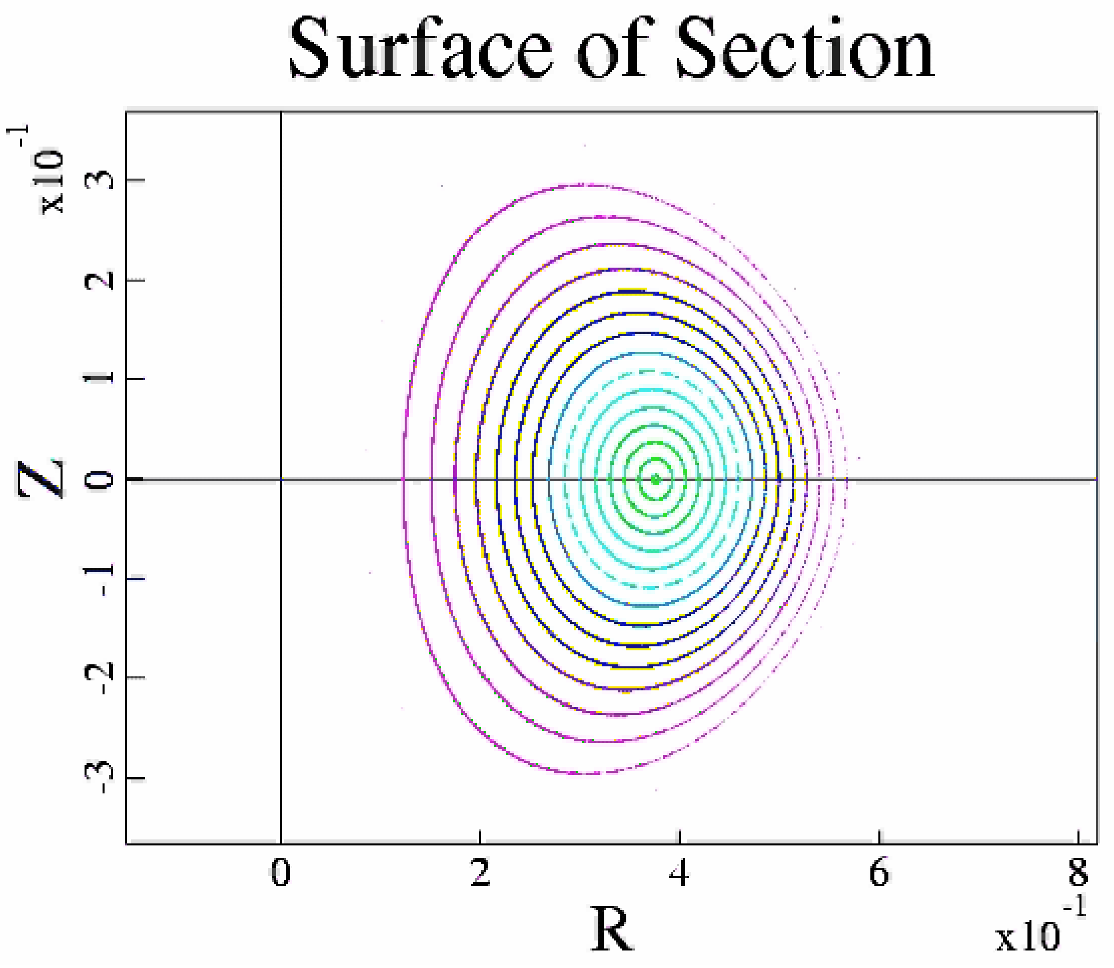

Schnack
Pankin

Calculation is being redone with 43 toroidal modes, and with $\kappa_{\perp}$=200m^2/s

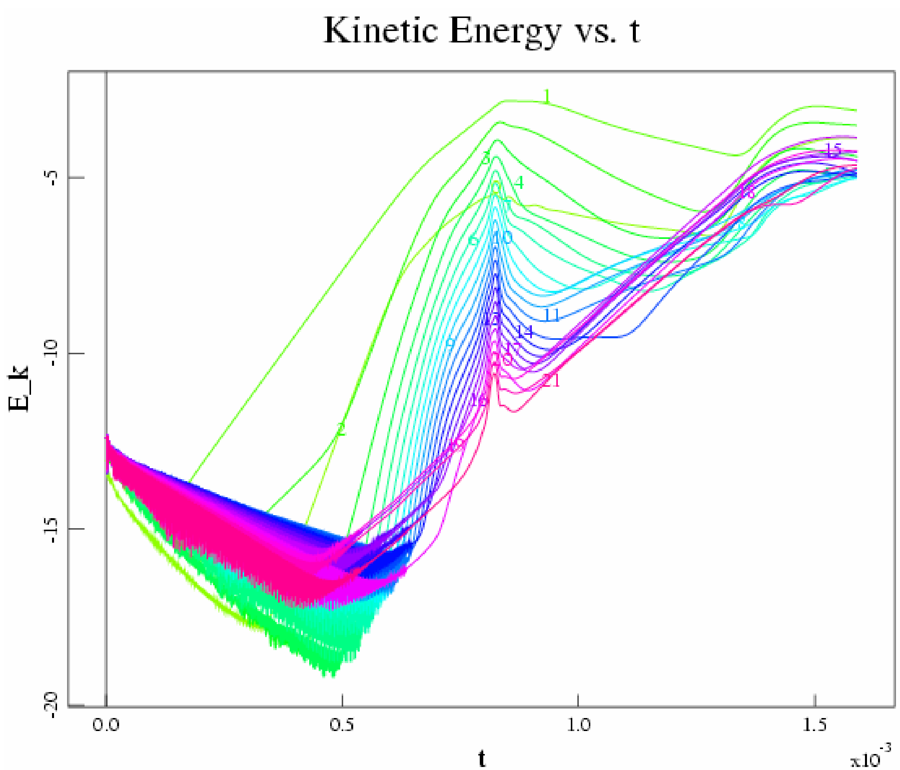

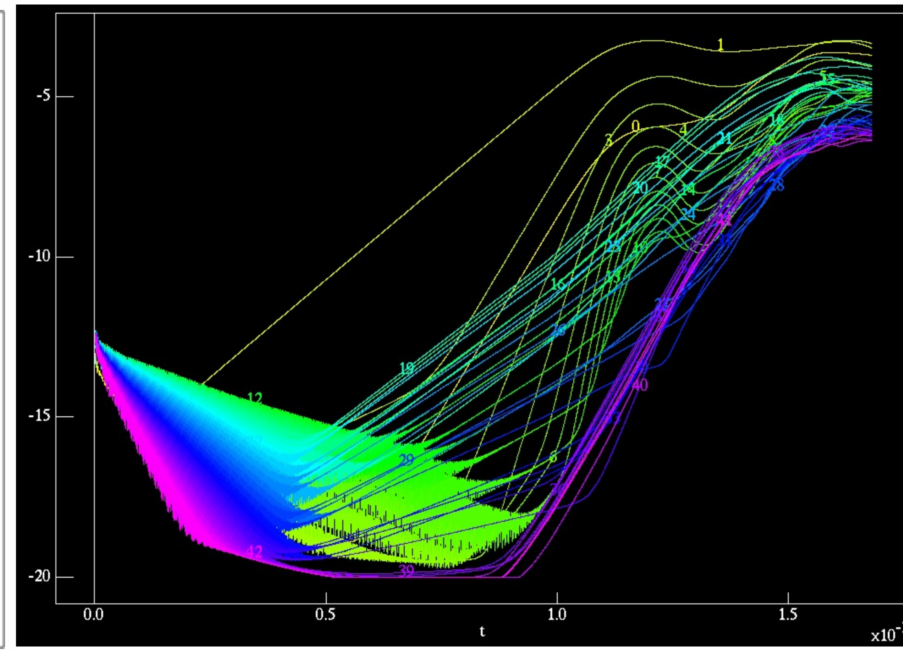

22 toroidal modes.

43 toroidal modes.

N=1 near full reconnection.

N=2-10 primarily nonlinearly driven

N=11-30 linearly unstable

N=31-43 nonlinearly driven

Schnack
Pankin

Conclusions of CDX-U Sawtooth Comparison

- Nonlinear MHD simulation with actual device parameters is capable of tracking evolution through repeated sawtooth reconnection cycles.

- M3D and NIMROD codes give same linear mode structures and growth rates, and qualitatively similar nonlinear behavior

- Quantitative comparisons with experimental data will require more careful attention to assumptions of the model.
  - Loop voltage (Ohmic) current drive in device vs. current source term in code.
  - Self-consistent Ohmic heating and evolving resistivity profile must be implemented.
  - Inclusion of two-fluid terms is likely to alter time and space scales of the sawtooth reconnection events.

Activity Areas

- Spatial Discretizations
  - M3D C^1
  - Spectral and lumped mass elements
- Two-Fluid MHD and Associated Temporal Differencing
- Numerical Closures
- Sawtooth Modeling
- ELM Modeling
- Hybrid Calculations
- Adaptive Mesh Refinement
- Spheromak Modeling
- 2-fluid NSTX Modeling
- Visualization
- Misc.

NIMROD has calculated linear and non-linear ELM evolution and compared with ELITE

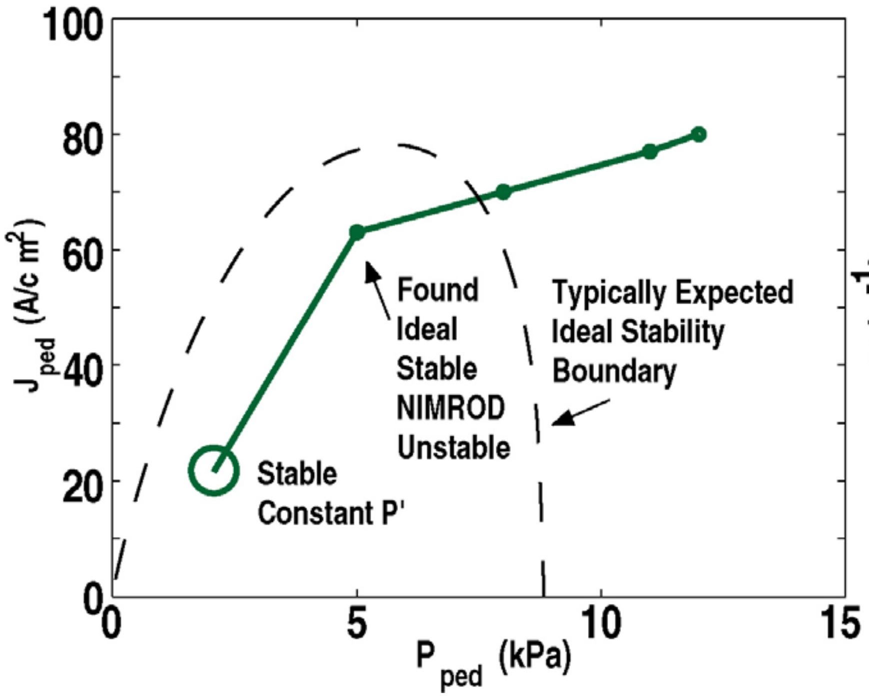

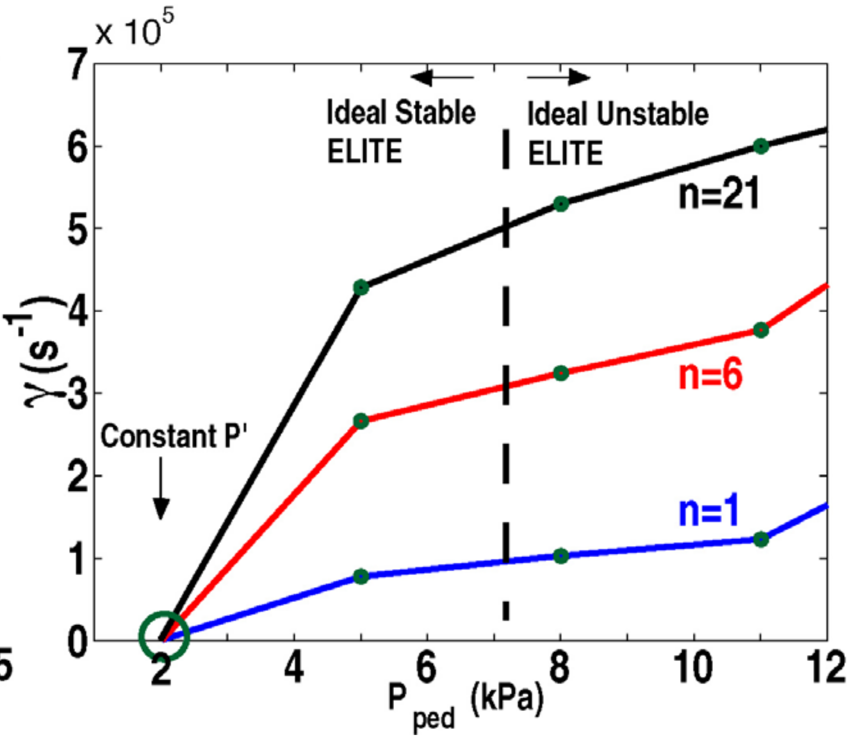

- NIMROD finds a “resistive” ELM unstable in the region ELITE finds stable
- Experiment resides near and crosses stability boundary during ELM cycle
- NIMROD → ELITE results when resistivity, viscosity → zero

Brennan,
Kruger

Poloidal Eigenmode Distribution Varies with n

- Low n modes have structure peaking top and bottom
- High n modes peak outboard midplane
- These differences affect nonlinear evolution
- Good agreement with ELITE in mode structure

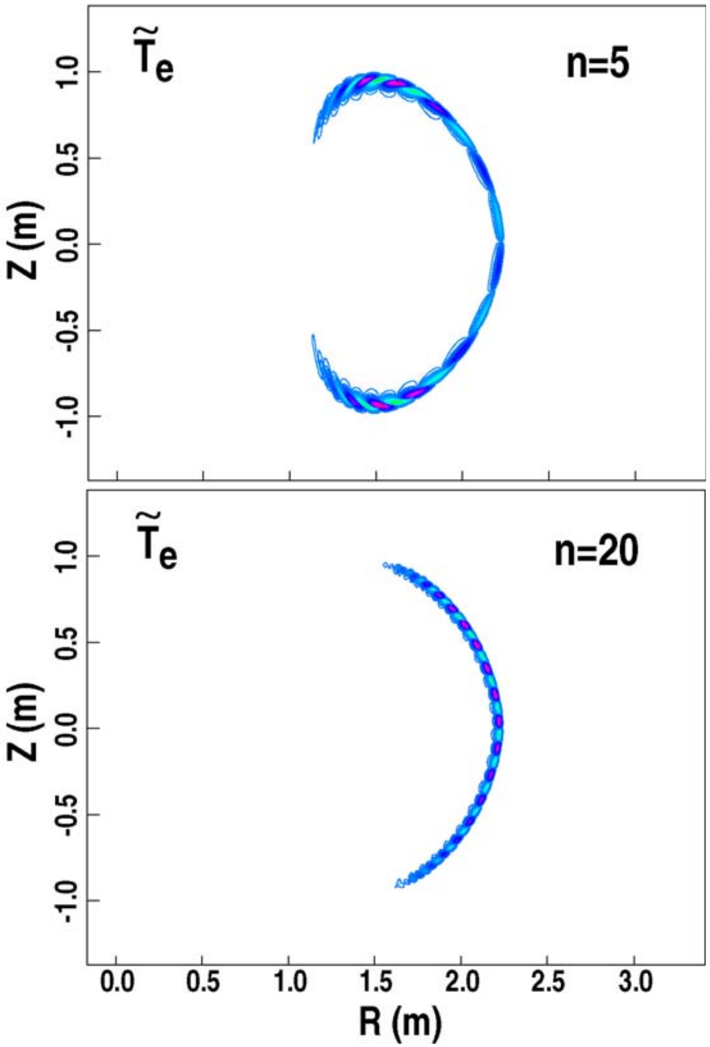

Brennan,
Kruger

Nonlinear ELM Simulation

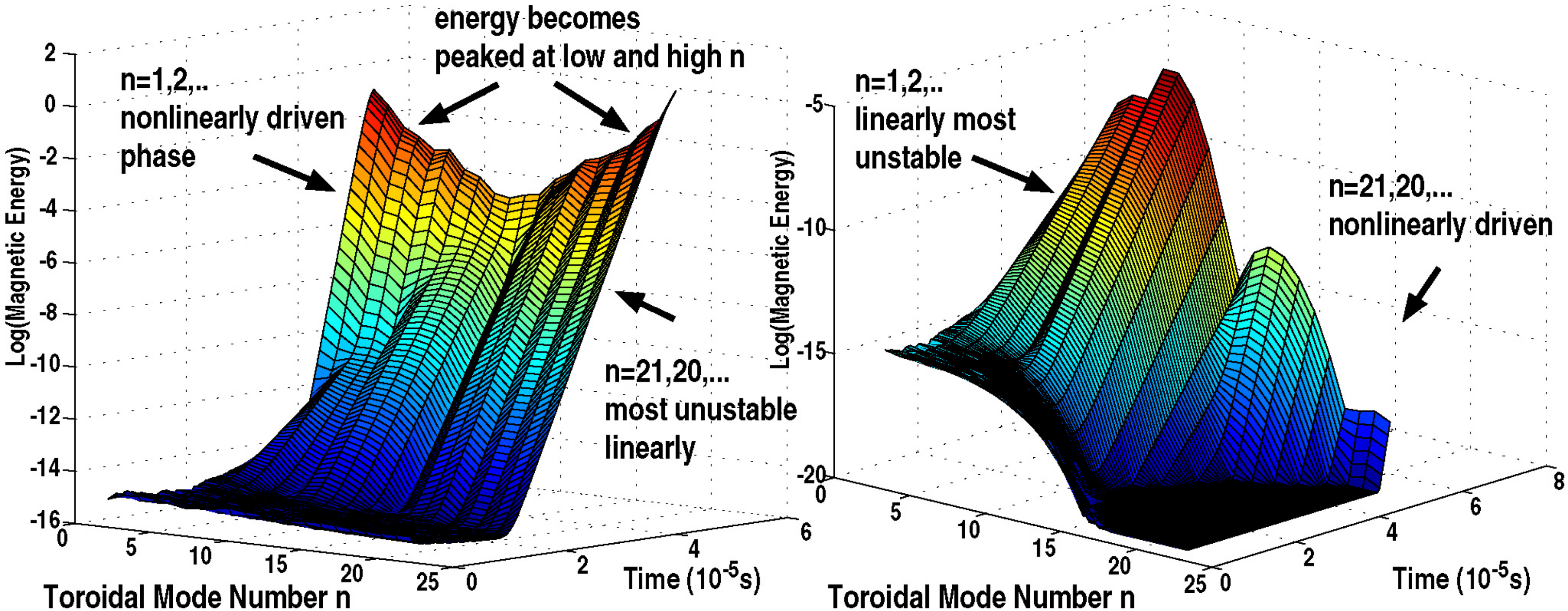

- **ELM evolution depends sensitively on relative initial mode amplitudes**
- **Implies need for accurate determination of stability onset for each of the different modes.**
- **Note that if all modes are initialized at the same amplitude, the highest modes grow to the largest amplitude, and the calculation is not resolved...**
    - **indicates need for improved model at high-n and/or more resolution**

Brennan,
Kruger

Resulting Nonlinear Perturbations Very Different Depending on Linear Spectrum

- **With HIGH-n dominance, mode is peaked outboard midplane.**
- **With LOW-n dominance mode is peaked top and bottom**

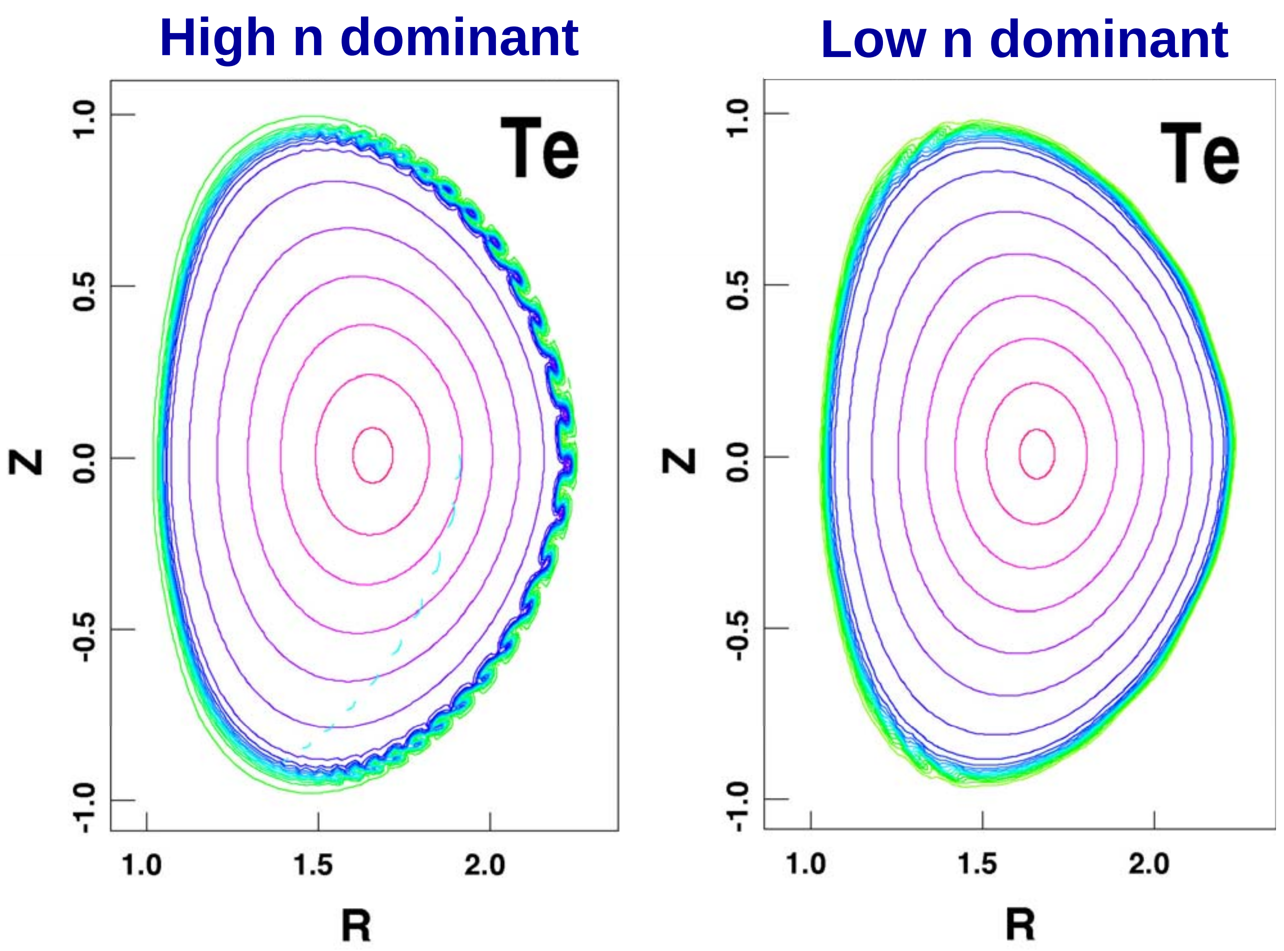

Brennan, Kruger

High-n dominated simulations show structure where high n linear modes peak

- The coupled modes form complex structures in flow velocity and Temperature, among other fields
- Areas of high temperature are seen flowing out and rotating, with blobs separating off on top and bottom

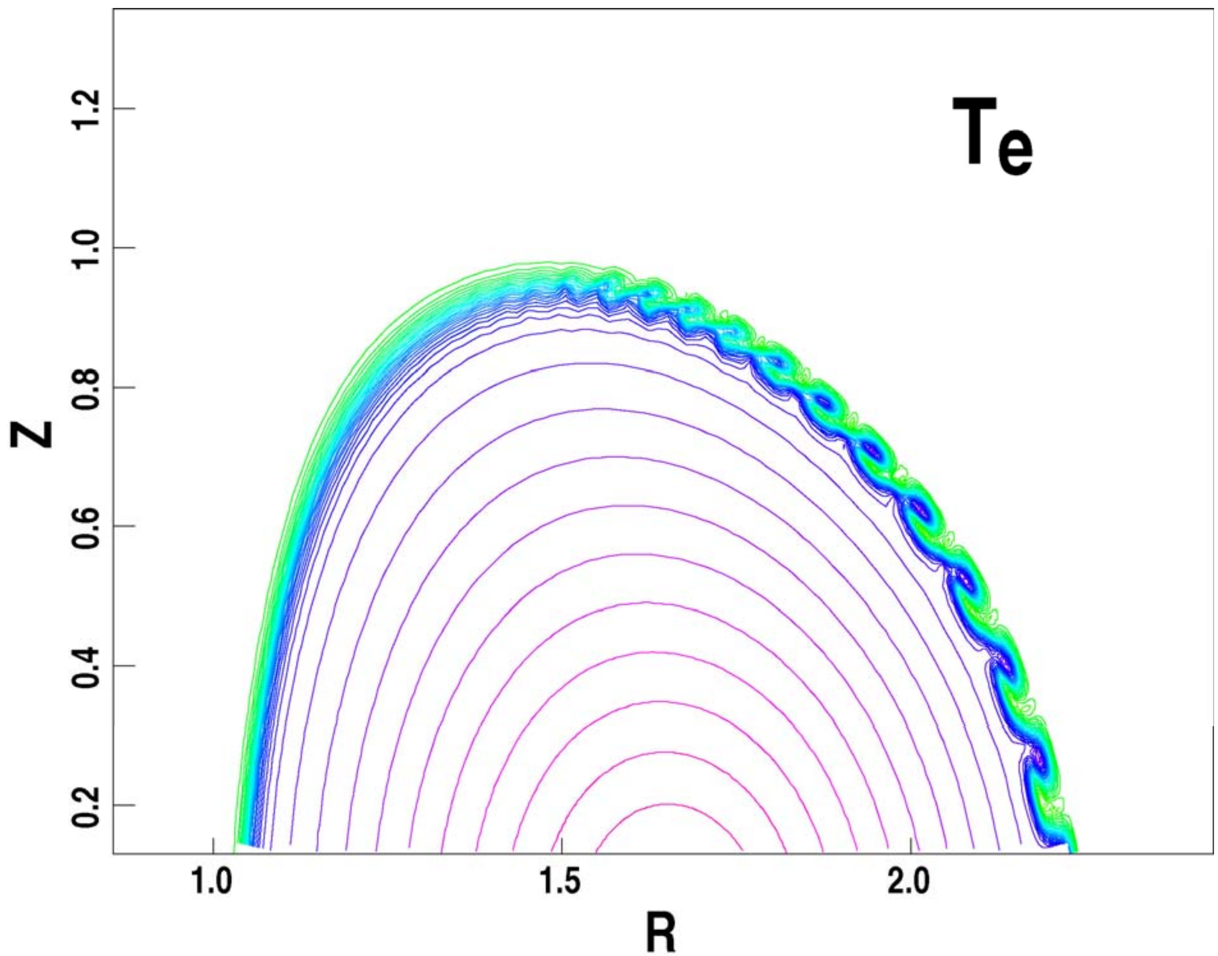

Brennan, Kruger

Low n dominated simulation shows structure where low-n linear modes peak

- **Although low-n dominant, still challenging to simulate into late nonlinear phase.**
- **Short wavelength blob structures form and propagate radially and poloidally, slowing time advance**

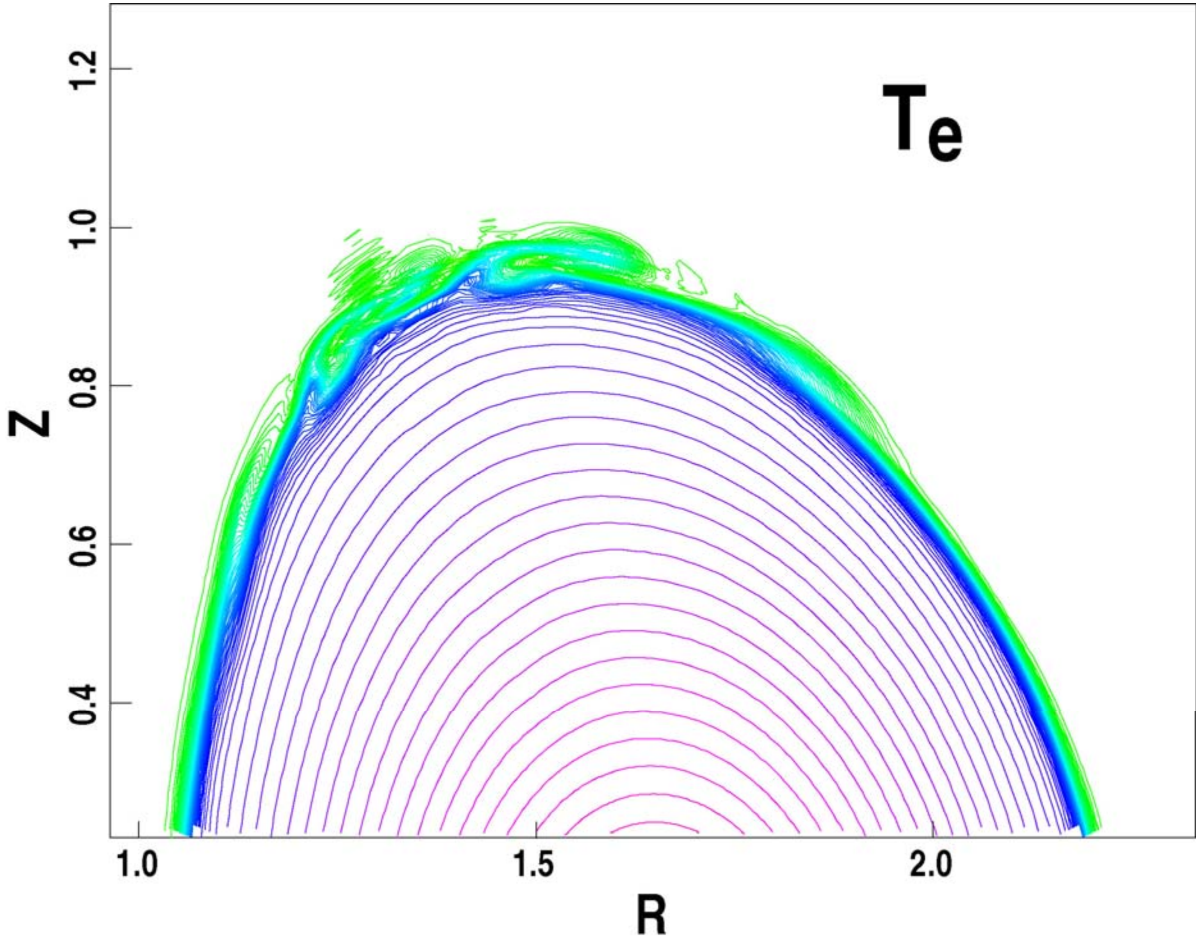

- **Numerically challenging to accurately resolve short wavelength driven components late into the nonlinear phase**

Brennan, Kruger

Nonlinear pressure evolution of an unstable ELM

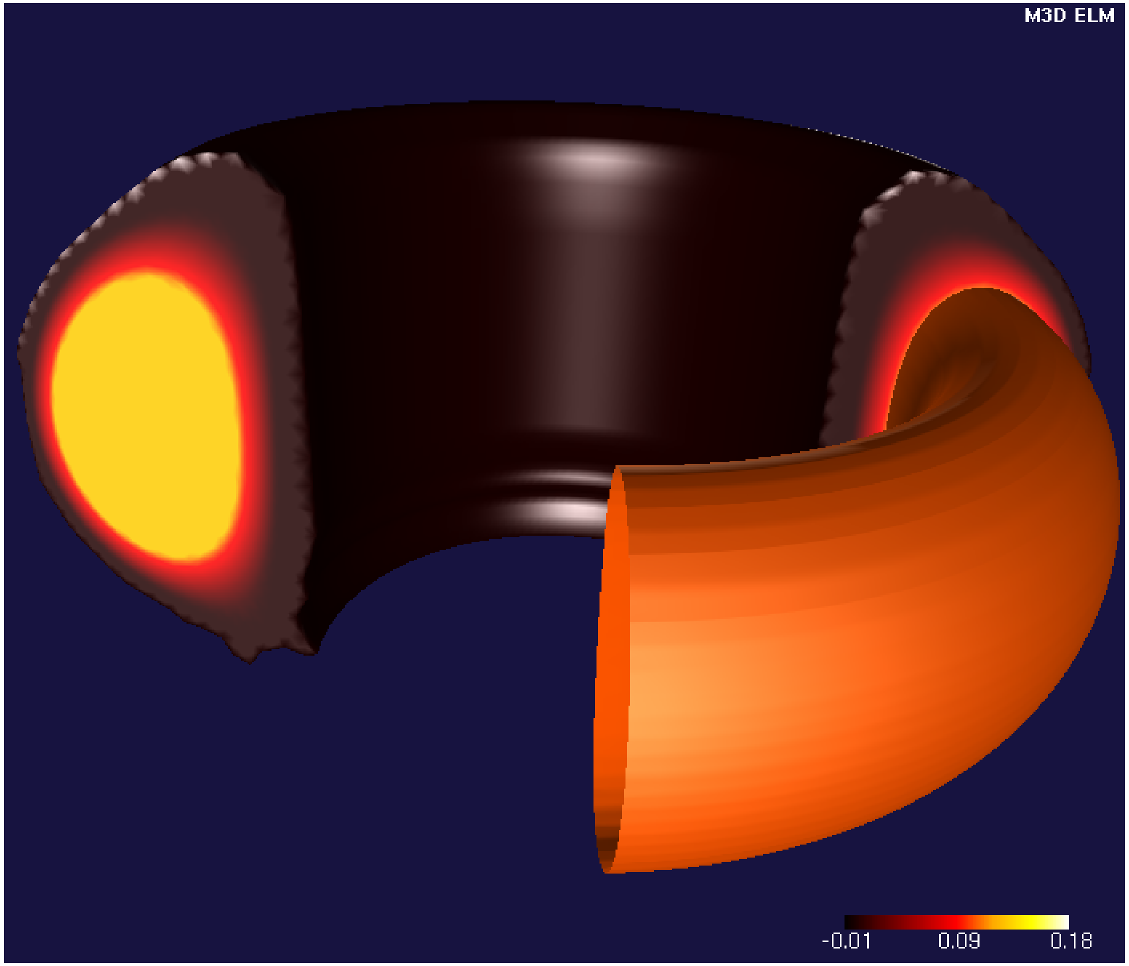

- M3D scoping runs were done with 16 planes, limited to n < 8. Uses 2^{nd} order spectral finite elements.

Strauss,
Klasky
(M3D)

Activity Areas

- Spatial Discretizations
  - M3D C^1
  - Spectral and lumped mass elements
- Two-Fluid MHD and Associated Temporal Differencing
- Numerical Closures
- Sawtooth Modeling
- ELM Modeling
- Hybrid Calculations
- Adaptive Mesh Refinement
- Spheromak Modeling
- 2-fluid NSTX Modeling
- Visualization
- Misc.

NIMROD and M3D now agree for linear growth rate of energetic particle test case

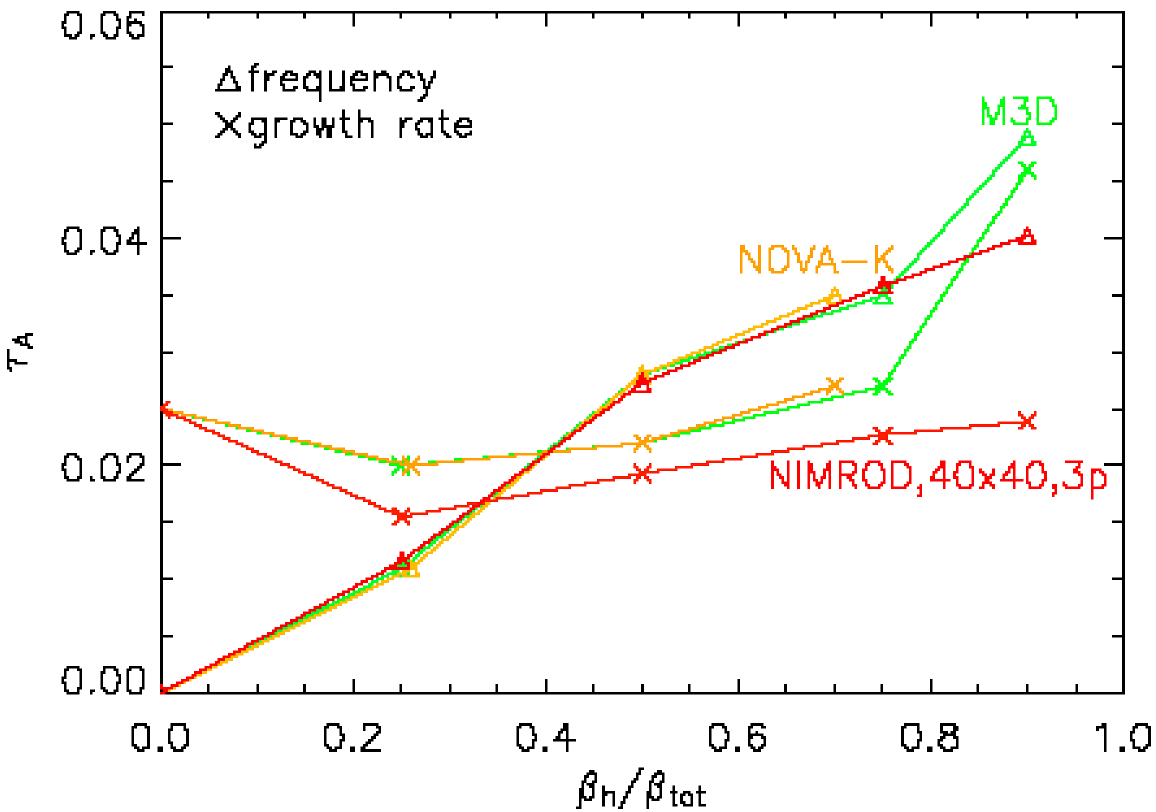

β_h varies at constant $\beta_T=\beta_h+\beta_P$

Kim, Fu

Excitation of Fishbone at high β_h

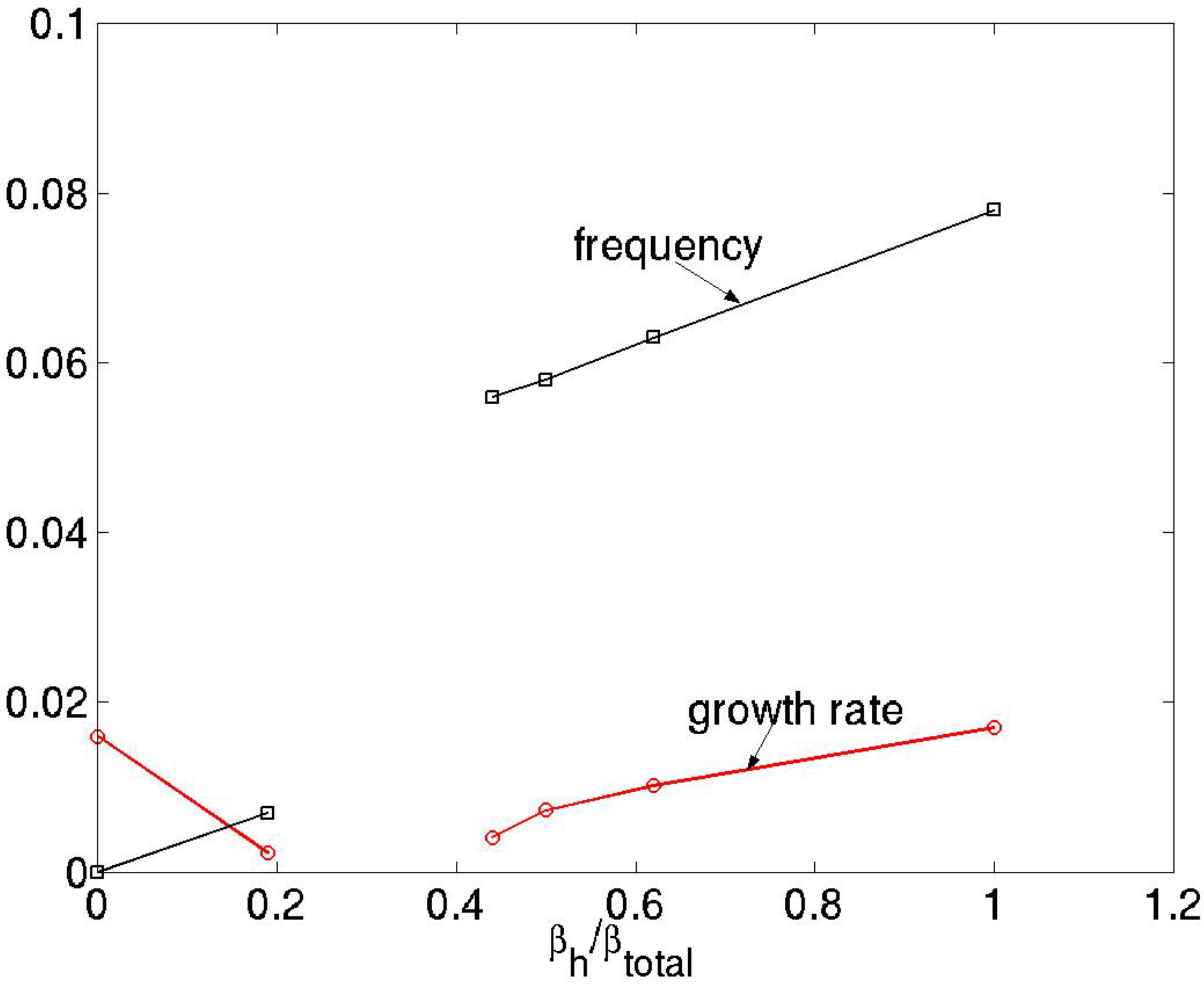

Circular
R/a=2.76
q(0)=0.9,
q(a)=2.5
β_(0) = 5.7%

Fu

Mode Structure: Ideal Kink v.s. Fishbone

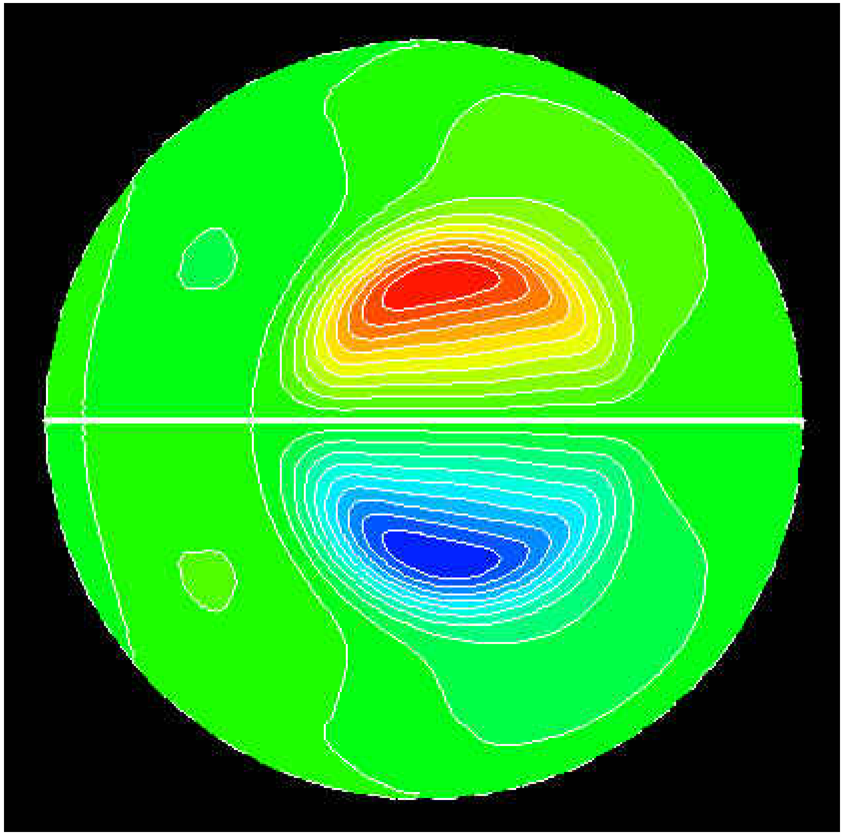

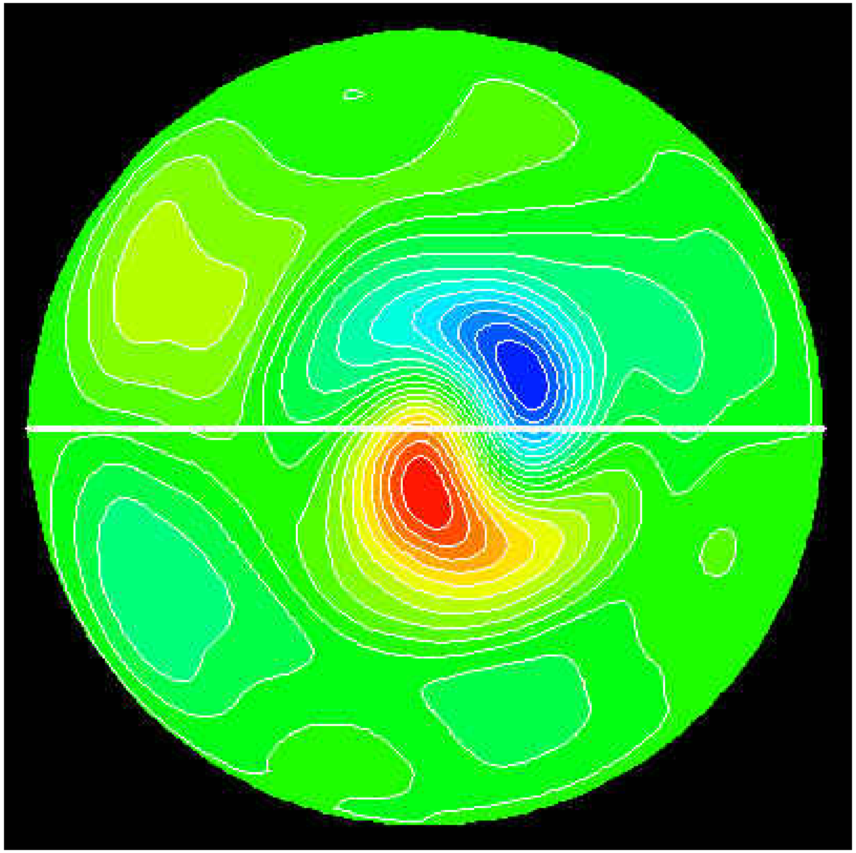

As flattening region of distribution function increases, the mode frequency chirps down.

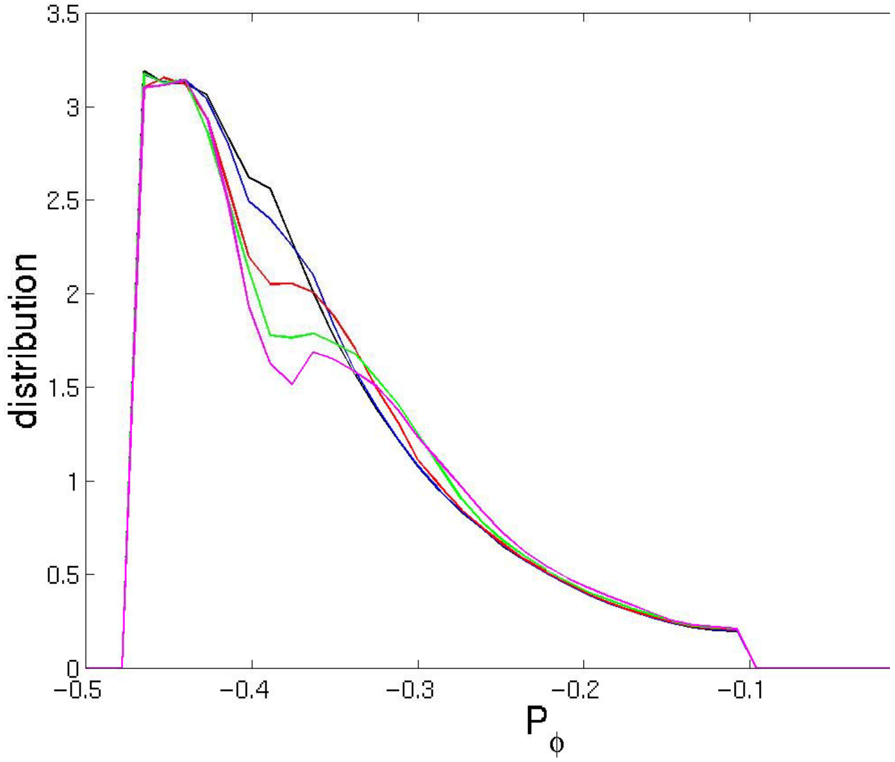

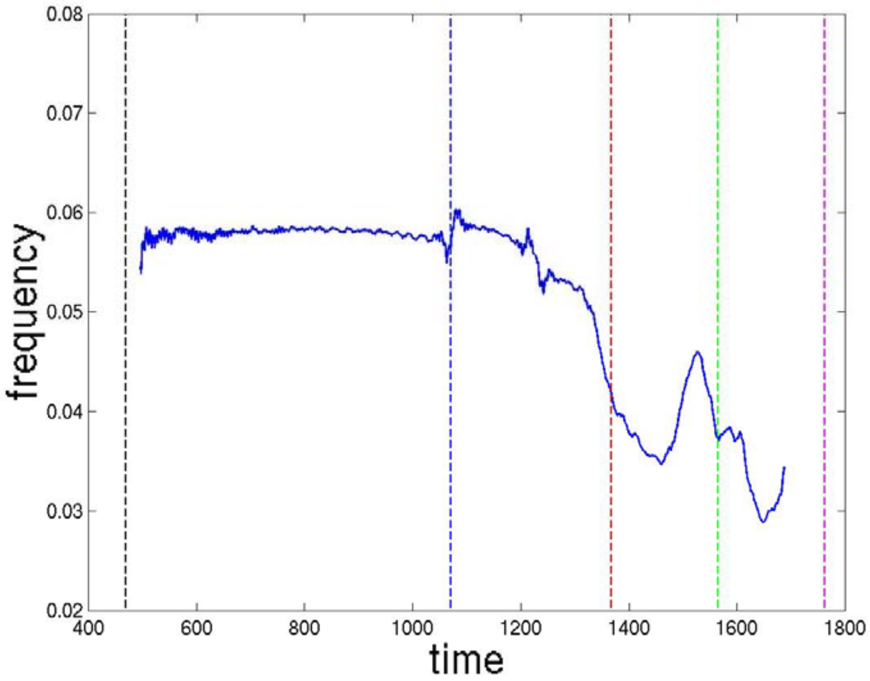

Fu

MHD nonlinearity changes mode structure significantly

Linear MHD

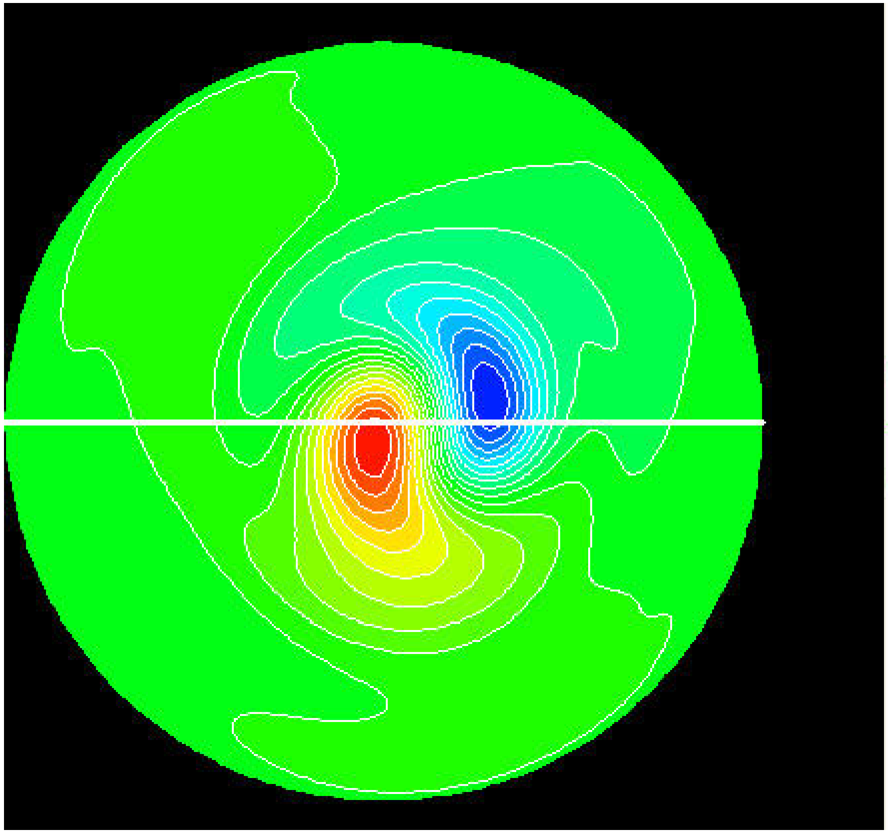

Nonlinear MHD

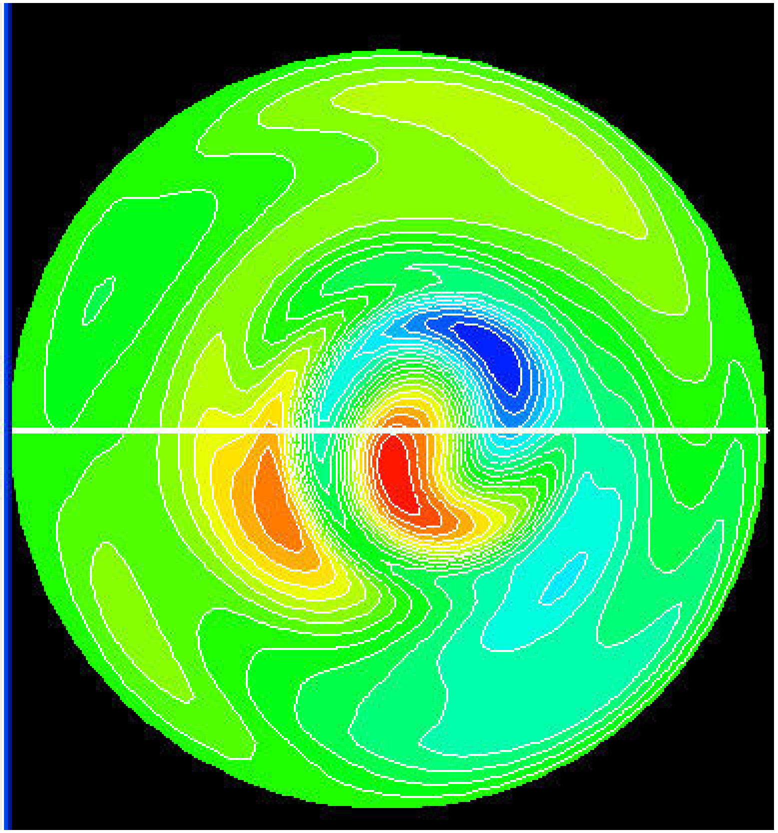

Fu

Activity Areas

- Spatial Discretizations
  - M3D C^1
  - Spectral and lumped mass elements
- Two-Fluid MHD and Associated Temporal Differencing
- Numerical Closures
- Sawtooth Modeling
- ELM Modeling
- Hybrid Calculations
- Adaptive Mesh Refinement
- Spheromak Modeling
- 2-fluid NSTX Modeling
- Visualization
- Misc.

AMR MHD Code: Recent Developments

- **We have implemented a non-orthogonal magnetic coordinate system in the AMR code**
  - Conservative finite volume upwind numerical method
  - The solenoidal condition on B is imposed using the *Central Difference* version of Constrained Transport (Toth JCP 161, 2000)
- **Handling of electron heat flux:**
  - Now have $\nabla_{||}T=0$ (Equilibration of temperature on flux surface)
  - Electron heat flux model by Ishizaki, Parks et al. (Phys. Plasmas 2004) is currently being implemented
- **Initial Conditions:**
  - Initial state is an MHD equilibrium obtained from JSOLVER equilibrium code
  - Input equilibrium for finest level and compute the metric terms
- **Boundary Conditions**:
  - Perfectly conducting for $\xi=\xi_o$, zero flux (due to zero area) at $\xi=\xi_i$, and periodic in θ and ϕ
  - Implementation results in preservation of volume and face areas of hexahedra upon refinement or coarsening
- **Pellet Injection**:
  - Ablation model of Kuteev (Nucl. Fusion 1995) used.
  - Supersonic gas jet injection being looked at.

R. Samtaney with
APDEC center:
P. Colella, D. Reynolds

Pellet Injection: HFS vs LFS Launch

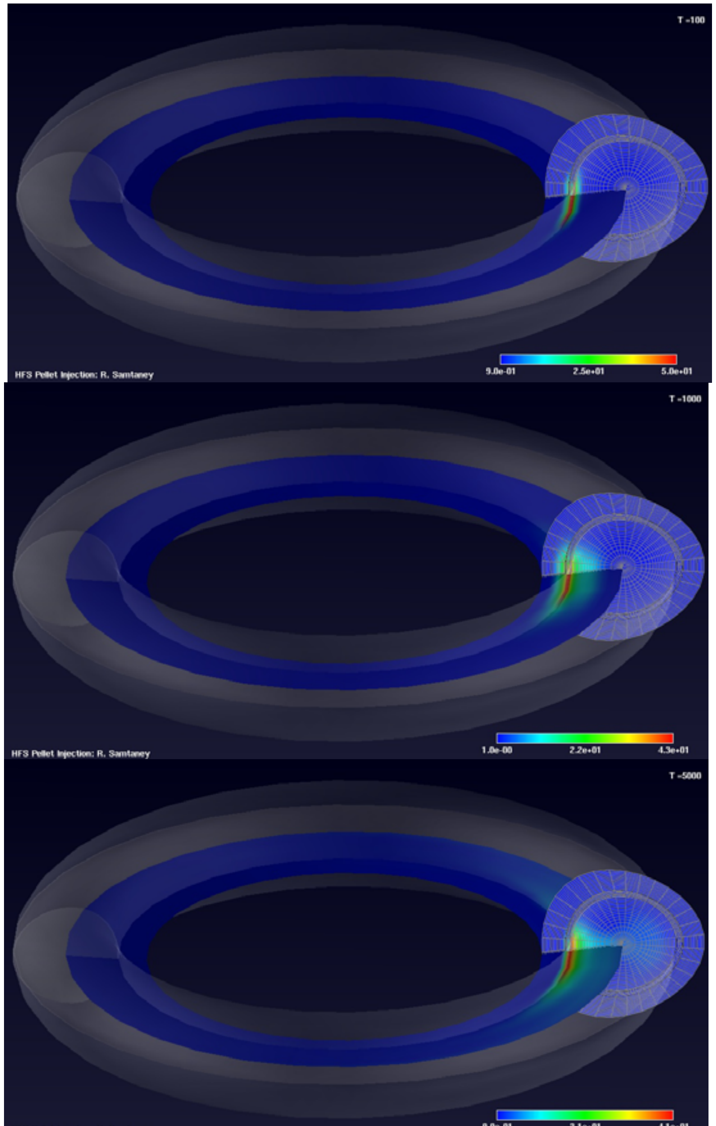

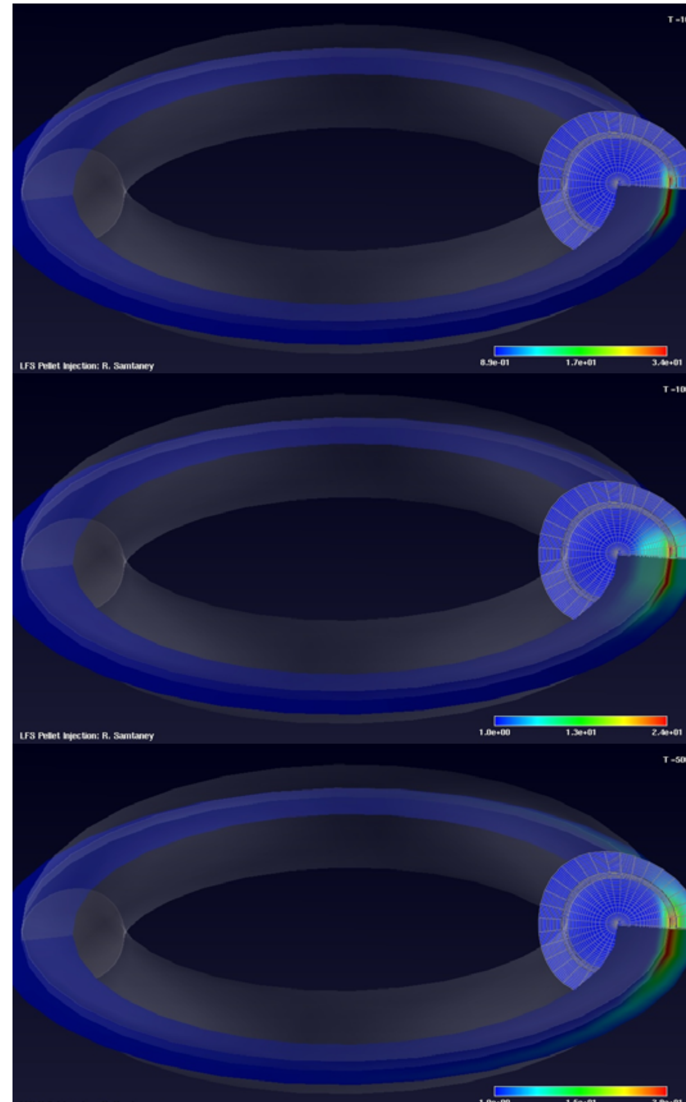

Density

R. Samtaney

Activity Areas

- Spatial Discretizations
  - M3D C^1
  - Spectral and lumped mass elements
- Two-Fluid MHD and Associated Temporal Differencing
- Numerical Closures
- Sawtooth Modeling
- ELM Modeling
- Hybrid Calculations
- Adaptive Mesh Refinement
- Spheromak Modeling
- 2-fluid NSTX Modeling
- Visualization
- Misc.

Success in the modeling of SPX with NIMROD has led to the use of NIMROD to model a proposed capacitor bank upgrade

Gun voltage

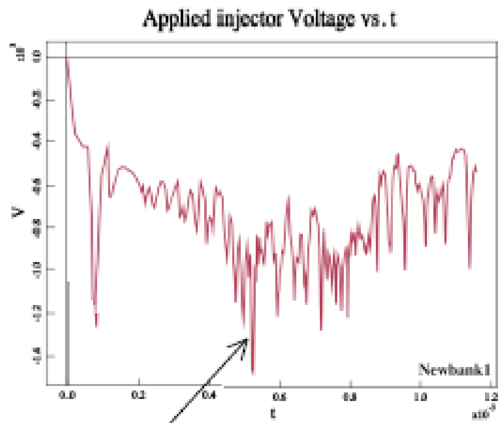

Gun current

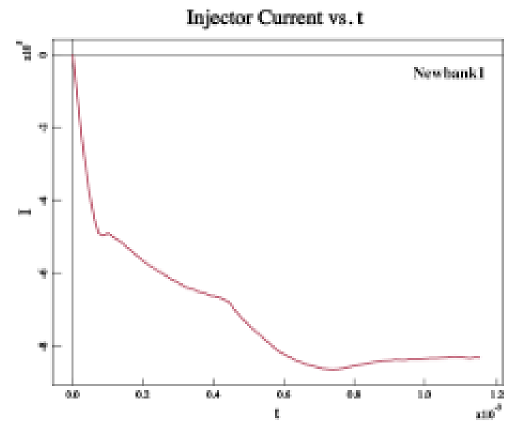

Voltage spikes are generated by magnetic reconnection events

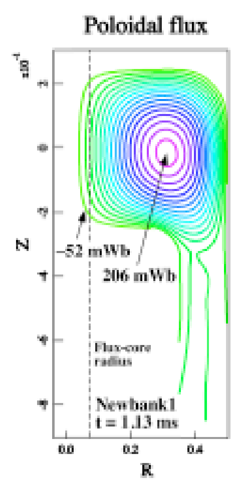

Azimuthally-averaged poloidal flux

Azimuthally-averaged poloidal flux is developed during this process, and a good mean-field spheromak has been produced

(Poloidal flux shown at t = 1.13 ms)

Detailed circuit equations included

Cohen, Hooper, Sovinec

Activity Areas

- Spatial Discretizations
  - M3D C^1
  - Spectral and lumped mass elements
- Two-Fluid MHD and Associated Temporal Differencing
- Numerical Closures
- Sawtooth Modeling
- ELM Modeling
- Hybrid Calculations
- Adaptive Mesh Refinement
- Spheromak Modeling
- 2-fluid NSTX Modeling
- Visualization
- Misc.

Temperature

2-fluid modeling with strong toroidal rotation is in qualitative agreement with recent NSTX results: long-lived saturated n=1 mode with co-injection

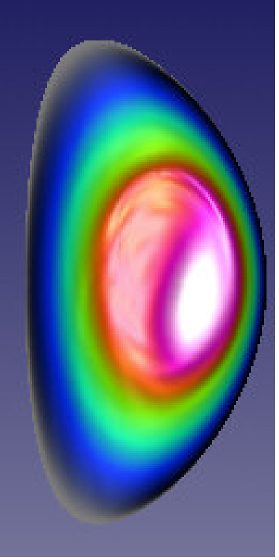

MHD

M_A=+-0.3

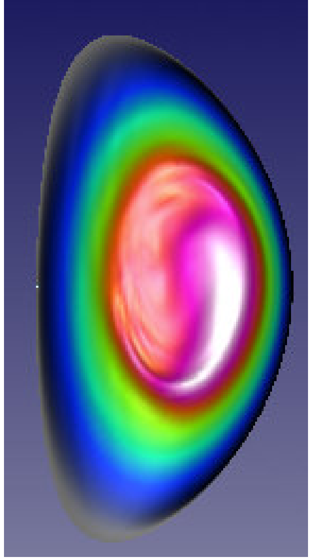

Counter 2Fuids

M_A=-0.3

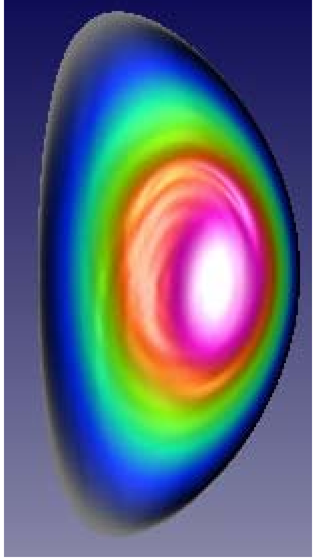

Co 2Fuids

M_A=+0.3

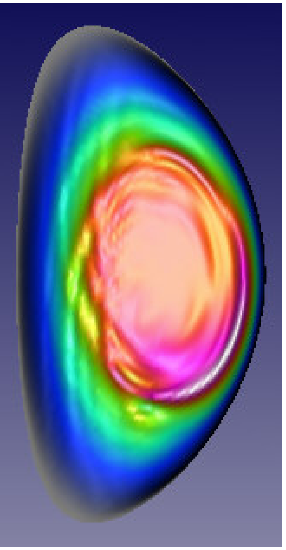

Crash

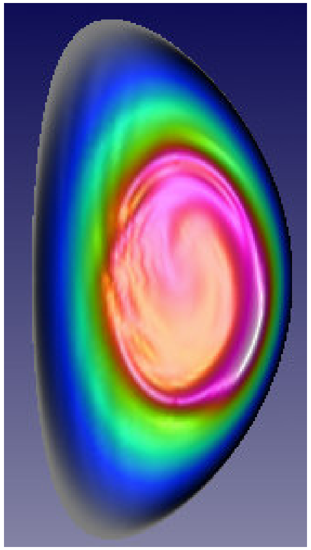

Crash faster than MHD case

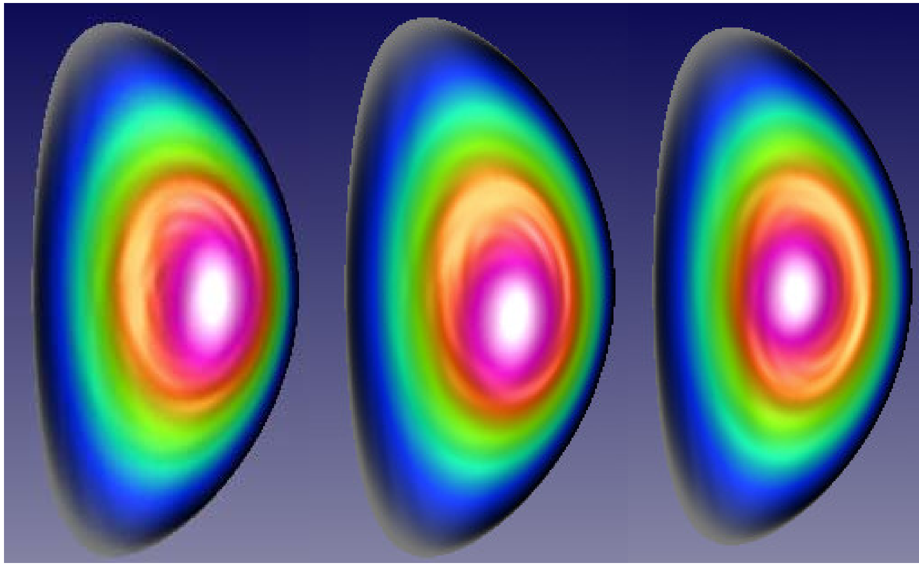

Saturation with hot spot pulled away from x-point

Park

M3D simulations examining role of η_{plasma} and rotation

Resistive plasma / resistive wall mode (RPRWM) growth rate scaling:

$\gamma \sim \eta^{1/3}\eta_w^{4/9}$ similar to analytic scaling

Finn 1995; Betti 1998

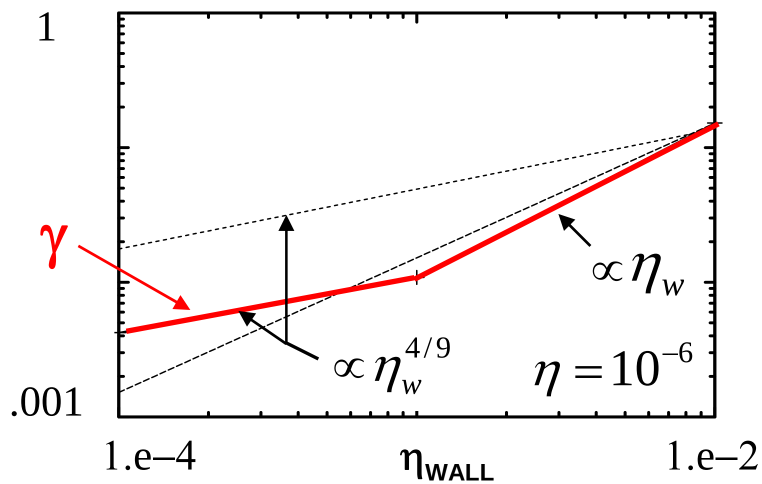

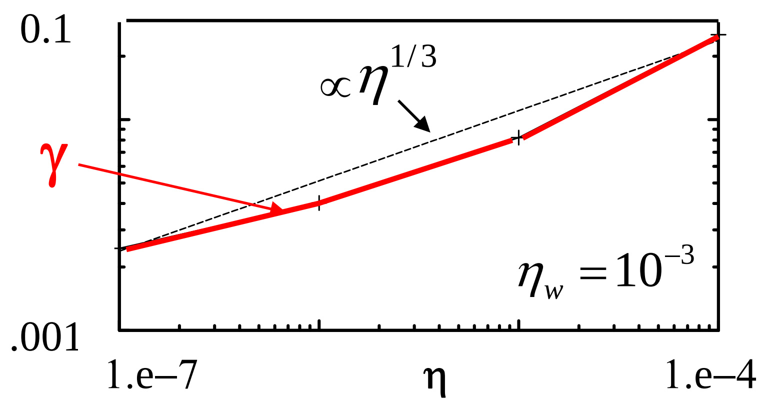

$\beta_N = 5, q_0 = 1.7$

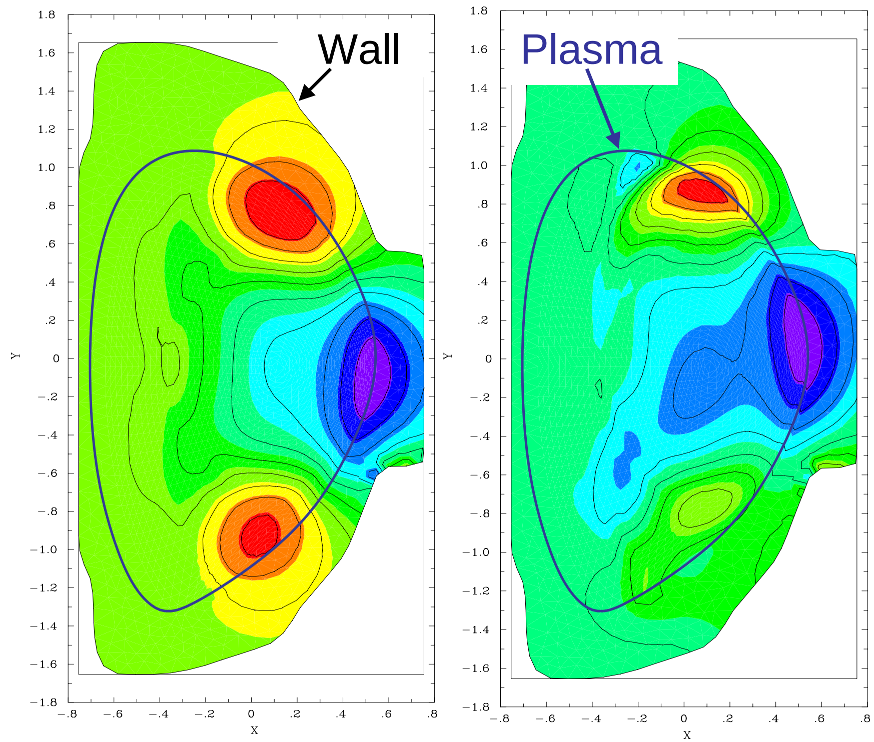

Perturbed Poloidal flux at $\Omega = 0$

Saturates at $\Omega = 0.05\frac{v_A}{R}$ w/ collisional viscosity

RWM interacts w/ tearing / EM η-ballooning mode

Better dissipation models needed

Strauss

Activity Areas

- Spatial Discretizations
  - M3D C^1
  - Spectral and lumped mass elements
- Two-Fluid MHD and Associated Temporal Differencing
- Numerical Closures
- Sawtooth Modeling
- ELM Modeling
- Hybrid Calculations
- Adaptive Mesh Refinement
- Spheromak Modeling
- 2-fluid NSTX Modeling
- Visualization
- Misc.

CEMM Visualization highlights

- Made the Integrated Visualization Development Environment more robust.
- Improved user interface
- Support more platforms (Altix, 64-bit linux, 32-bit linux, windows, MAC).
  - drop down menus, scrollbars, better tick marks, more colormaps,…)
- Multiple bug fixes
- New routines: toroidal geometry recognition, …

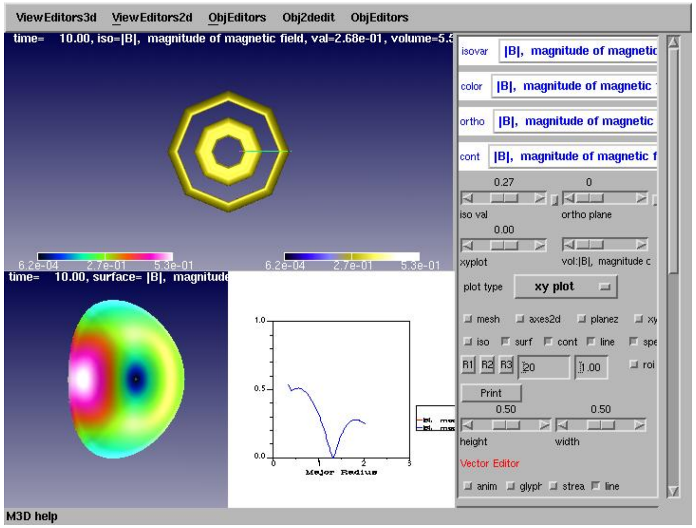

Without toroidal geometry recognition

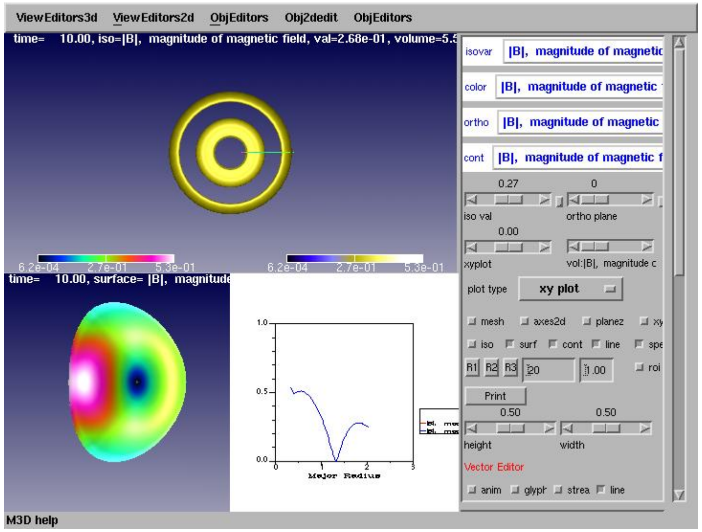

Toroidal geometry recognition

Advanced Viz. Research Topics

- Detection of critical points
  - (B Field and velocity).
- Tracking of critical points
  - (B Field and velocity).
- Detection of closed field lines
  - (B Field only).

- Tasked for completion at one per year.

Critical Points - Plasma Velocity

- LIC - Line Integral Convolution in the plane shows the swirling nature of the flow.
- Color mapping shows the flow into (red) and out of blue) the plane.
- White contours are locations where the flow is solely in the plane.

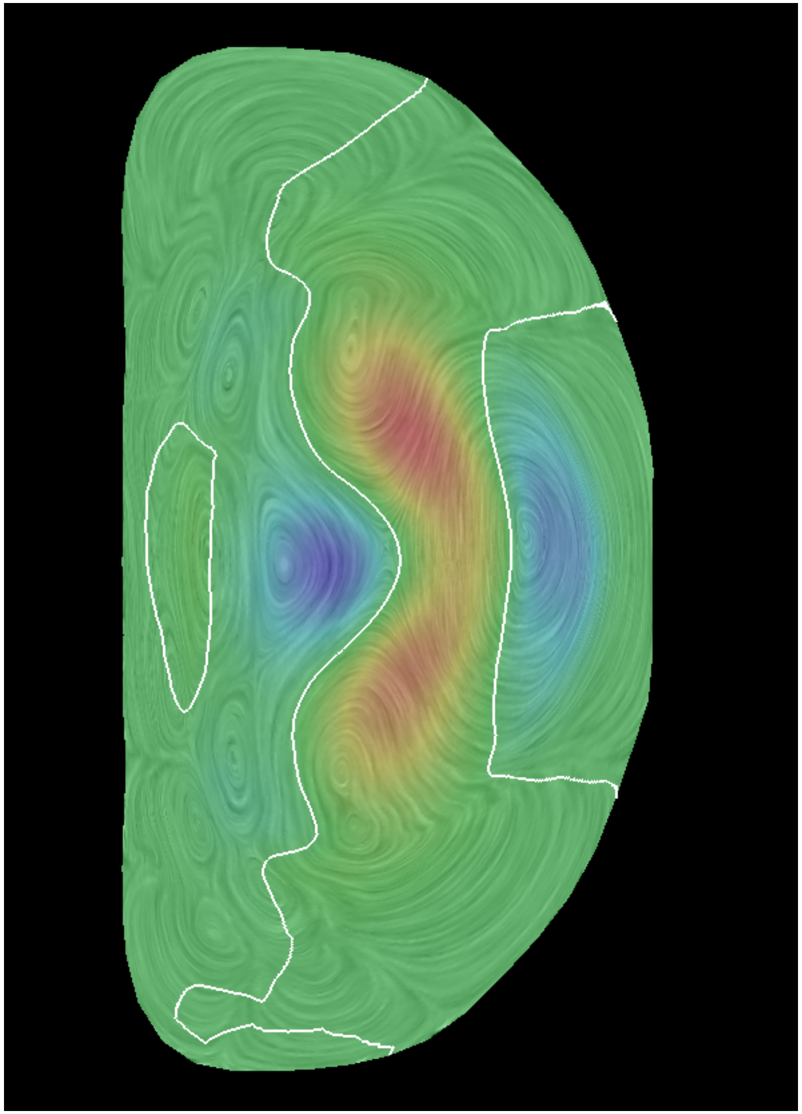

Sanderson

Activity Areas

- Spatial Discretizations
  - M3D C^1
  - Spectral and lumped mass elements
- Two-Fluid MHD and Associated Temporal Differencing
- Numerical Closures
- Sawtooth Modeling
- ELM Modeling
- Hybrid Calculations
- Adaptive Mesh Refinement
- Spheromak Modeling
- 2-fluid NSTX modeling
- Visualization
- Misc.

Other Activities

TSTT Collaboration:

- Working with the SCOREC Center at RPI to interface an adaptive meshing algorithm with the M3D-C^1 code

A. Bauer, M. Sheppard

TOPS Collaboration:

- Have sped up M3D by a factor of 2 by further analysis of the 13 sparse matrix solves that are performed each time step.
  - Different operators and boundary conditions
  - Now use different methods on different equations:
    - Congugate gradient with Jacobi preconditioner
    - Congugate gradient with hypre (multi-grid) preconditioner
    - GMRES with ILU preconditioner

Mark Adams, Jin Chen, David Keyes

Future Activities

- Closure workshops and activities
  - Summer 2-day closure meeting attached to NIMROD meeting
  - Expanded (1 ½ day) pre-APS CEMM meeting
  - Larger workshop Spring 2006
  - Goal is to identify sequence of test problems
- Working towards burning plasma problems
  - 7 critical problems identified that are of interest to ITER
    - (sawtooth, NTM, RWM, EPM, ELM, VDE, fueling)
- Improve infrastructure
  - Further expand common visualization packages
  - Unified data management system
- Integration Activities
  - Integrated calculation with RF group
  - Hybrid calculation of neoclassical closures
  - Interaction with Edge FII